minerals

MDPI

Article

Origin of Diorites and Coeval Mafic Microgranular Enclaves in the Liuba Region, South Qinling Orogen, Central China: Insights from Petrography, Zircon U-Pb Geochronology and Geochemistry

Shan Gao [1], Xianzhi Pei [1,2,*], Lei Pei [1,2], Zuochen Li [1,2], Ruibao Li [1,2], Shaowei Zhao [1,2], Mao Wang [1], Li Qin [1] and Xiao Wang [1]

[1] School of Earth Sciences and Resources, Chang'an University, Xi'an 710054, China; gaoshan3051337085@163.com (S.G.); peilei.1989@163.com (L.P.); lizuochen@chd.edu.cn (Z.L.); li-ruibao0971@163.com (R.L.); shwzhaoqx@163.com (S.Z.); wmchd_0908@163.com (M.W.); qinlichd@163.com (L.Q.); wx981098@163.com (X.W.)

[2] Key Laboratory of Mineral Resources and Geological Engineering in Western China, Ministry of Education, Xi'an 710054, China

* Correspondence: peixzh@163.com

Abstract: The formation of early Mesozoic granitoid plutons in the Qinling Orogen is widely regarded as a result of the collision and accretion between the Yangtze Block and the South Qinling Block during the early Mesozoic, but the specific magmatic process, source composition, tectonic environment and deep dynamic background remain controversial. This study reports the petrology, zircon U–Pb geochronology, and whole-rock geochemistry of diorites from the Liuba and Qingyangyi plutons in the South Qinling, to provide new evidence for understanding the final collision tectonic evolution process of Qinling Orogenic belt. The Liuba and Qingyangyi plutons, located in the central part of the South Qinling region, are primarily composed of quartz diorite and quartz monzodiorite, respectively. The results indicate that the weighted mean crystallization ages of the quartz diorite in the Liuba pluton range from 216.1 ± 0.8 Ma to 217.1 ± 1.3 Ma, with the weighted mean crystallization ages of its MMEs being 215.4 ± 1.0 Ma. The crystallization ages of the quartz monzodiorite in the Qingyangyi pluton range from 214.6 ± 0.9 Ma to 215.4 ± 0.9 Ma, suggesting that both plutons were formed in the late Triassic. The investigated plutons are characterized as right-leaning and have weak negative Eu anomalies on the chondrite-normalized REE patterns diagram. The large ion lithophile elements (LILE) Rb, Ba, Th and K are relatively enriched, while high-field strength elements (HFSE) Nb, Ta, Ti and P are strongly depleted. The formation of numerous MMEs in the Liuba pluton is the product of magmatic mixing. The Liuba and Qingyangyi plutons are the results of crust thickening and partial melting of lower crust caused by the comprehensive late Triassic collision between the Yangtze Block and the North China Block (NCB), and are the manifestation of magmatic intrusion along the South Qinling tectonic belt in the late Triassic period.

Keywords: South Qinling; Liuba pluton; Qingyangyi pluton; zircon U-Pb age; petrogenesis; MMEs

check for updates

Academic Editor: Giorgio Garuti

Received: 5 December 2024
Revised: 9 January 2025
Accepted: 11 January 2025
Published: 15 January 2025

Citation: Gao, S.; Pei, X.; Pei, L.; Li, Z.; Li, R.; Zhao, S.; Wang, M.; Qin, L.; Wang, X. Origin of Diorites and Coeval Mafic Microgranular Enclaves in the Liuba Region, South Qinling Orogen, Central China: Insights from Petrography, Zircon U-Pb Geochronology and Geochemistry. *Minerals* **2025**, *15*, 77. https://doi.org/10.3390/min15010077

Copyright: © 2025 by the authors. Licensee MDPI, Basel, Switzerland. This article is an open access article distributed under the terms and conditions of the Creative Commons Attribution (CC BY) license (https://creativecommons.org/licenses/by/4.0/).

1. Introduction

The Qinling Orogen is a composite continental orogen formed by the collision of the North China Block (NCB) and the Yangtze Block and has undergone the evolution of

different tectonic systems before forming the present basic tectonic framework [1–4]. The Qinling Orogen experienced a tectono-magmatic event related to block convergence and rifting, resulting in the formation of the syn-collision to post-collision granitic series [5,6]. In the Paleozoic, subduction–collision and accretion occurred along the Shangdan tectonic belt in the North Qinling, accompanied by a large amount of granitic magmatic activity [7]. The South Qinling area within the Qinling Orogen experienced a strong early Mesozoic tectono-magmatic event and, along the north side of the Mianlue tectonic belt, developed an east–west-trending late Triassic granite belt [2,8]. Among the most typical pluton groups are Dongjiangkou (Gaoqiaojie, Dongjiangkou, Zhashui, Caoping and Shahewan pluton), Wulong (Xiba, Huayang, Wulong, Laocheng, Xichahe and Yanzhiba pluton) and Guangtoushan (Miba, Xinyuan, Jiangjiaping, Zhangjiaba, Guangtoushan, Liuba pluton, Qingyangyi pluton). They appear as irregular, non-deformed elliptical large plutons exposed within Precambrian middle-to high-grade metamorphic rock series and Paleozoic lower-grade metamorphic strata [7]. This granite belt records important information about the formation and evolution of the Qinling Orogen. The study of the petrological, geochemical and chronological characteristics of these granitoid plutons is essential for reconstructing the tectonic evolution of the Qinling Orogen.

The Liuba and Qingyangyi plutons, which are located in the north side of the Mianlue tectonic belt in the South Qinling, are part of the granite belt. Through detailed geochemical and chronological studies, the tectonic properties of magmatic rocks are discussed, and the research results of magmatic rocks in the South Qinling tectonic belt are collected. By comparing the magmatic events on the northern and southern margin of the South Qinling tectonic belt and the peripheral land blocks, we can effectively constrain the formation and evolution of the Qinling Orogen and the collision process of the Yangtze Block and the NCB, thus providing new evidence for a comprehensive and in-depth understanding of the final collision and tectonic evolution process of the Qinling Orogen [9–11]. There are three major pluton groups of early Mesozoic granite in the South Qinling: the Guangtoushan pluton group, the Wulong pluton group and the Dongjiangkou pluton group, listed from west to east [7,12,13]. Although numerous studies have been carried out and important progress has been made, Liuba and Qingyangyi plutons have not received sufficient research attention, and related studies are relatively scarce. Previous data show that the Liuba and Qingyangyi plutons were formed in the Carboniferous period [14,15]; the formation age of these plutons is quite different from that of other nearby plutons. The obtained age of the surrounding plutons includes the Miba pluton 220 ± 2 Ma, Zhangjiaba pluton 219 ± 1 Ma, Xinyuan pluton 214 ± 1 Ma, Guangtoushan pluton 216 ± 2 Ma and Jiangjiaping pluton 206 ± 2 Ma [16], and the lithology of Liuba and Qingyangyi plutons are obviously different from those of other plutons in the field. In conclusion, the Liuba and Qingyangyi plutons and dark mafic microgranular enclaves (MMEs) of the Liuba pluton are selected for the study of chronology and geochemistry, and their petrogenesis, magmatic processes and tectonic environment are discussed, providing new geological evidence for the study of the early Mesozoic tectonic evolution of the Qinling orogen.

2. Geological Background

2.1. Geological Overview of the Study Area

The Qinling Orogen is located in central China (Figure 1a), spreading in a nearly east–west direction. The Qinling is a composite continental orogen formed by different tectonic regimes at different stages of development, and it is also the main north–south combined belt in the Chinese mainland, with a complex evolutionary history and tectonic pattern (Figure 1b) [4,10,17]. The Qinling Orogen underwent long-term, multi-stage development, beginning in the middle and late Neoproterozoic and culminating by the late Triassic [10].

After the Neoproterozoic orogeny, it experienced subduction–collision processes during the Paleozoic, and the orogen finally formed through an intense collision in the early Mesozoic [7,18,19]. According to studies in geology, geochemistry and geochronology, the Qinling Orogen progressively developed two tectonic belts: the Shangnan–Danfeng (Shangdan) tectonic belt in the northern part of South Qinling and the Mianxian–Lueyang (Mianlue) tectonic belt in the southern part, which together constructed the "three plates and two sutures" tectonic pattern [4,8,20–22]. The Shangdan tectonic belt is the main tectonic boundary in the Qinling region that marks the ocean–continent interaction during the early Paleozoic and the subsequent continental collision [2,3,5,23]. The Mianlue tectonic belt is the main tectonic belt in which the Qinling Microblock and the Yangtze Block completed the main amalgamation during the late Triassic period, and it is also the symbol of the comprehensive assembly and collision between the NCB and the Yangtze Block and the final formation of the major tectonic pattern of the Qinling Orogen [2,10,24,25]. In the early Neoproterozoic to Mesozoic period, the Qinling, as the northern branch of the Proto-Paleo-Tethys Ocean, developed and evolved into two finite oceans. These two main tectonic belts divided the Qinling Orogen into four tectonic units, respectively, the southern margin of the NCB, the North Qinling tectonic belt, the South Qinling tectonic belt and the northern margin of the Yangtze Block from north to south. These four tectonic units subducted and collided along the two main suture zones in the Caledonian plate, then the continental–continental collision and orogeny occurred successively in the late Devonian and late Triassic periods, and then due to the influence of the Meso-Cenozoic Himalayan Orogeny, in the late Jurassic to early Cretaceous, the present Qinling was formed through the evolution of intra-continental orogeny, intra-continental tectonics from the late Cretaceous to the Cenozoic, rapid uplift into mountains and new cracking structures.

The crystalline basement of the South Qinling mainly includes the Neoarchean–Paleoproterozoic Yudongzi complex, Foping complex and Douling complex, and the transitional basement of the South Qinling mainly includes the Neoproterozoic Wudang Group, Yaolinghe Group and other tectonic rock units. The sedimentary covers in the South Qinling are mainly sedimentary rock series from late Neoproterozoic to early Mesozoic [26], including the Sinian Doushantuo Formation and Dengying Formation. The early sedimentary facies are platform facies and shelf shallow marine clastic sedimentary facies, and the late epicontinental carbonate sedimentary facies [2].

Magmatic rocks are widely exposed in the South Qinling, mostly the late Triassic granites. The South Qinling granites are composed of multiple large complex pluton groups, including the Guangtoushan, Baoji, Huayang, Wulong, Dongjiangkou and other large pluton groups. The main rock types are granodiorite, quartz diorite, porphyritic granite and other medium-acid rocks. The available geochronological data indicate that the crystallization age of the late Triassic granite plutons in the South Qinling is concentrated in 200~230 Ma [7,16].

2.2. Local Geology

The study area is exposed in the Liuba region of Hanzhong in South Qinling and is geotectonically located between the Shangdan Suture Zone and the Mianlue Suture Zone (Figure 1b). The area mainly intrudes into the carbonaceous slate and metamorphic sandstone of the Zhouqu Formation, Bailongjiang Group, Silurian, and the rock type is mainly quartz diorite. A large number of MMEs have also developed in plutons. The Qingyangyi pluton is exposed to the southeast of the Liuba pluton and mainly intrudes in the carbonaceous slate of the Zhouqu Formation. The rock type is mainly quartz monzodiorite (Figure 1c). The magmatic activities in the region are mainly intermediate–acidic intrusive rocks of the late Triassic.

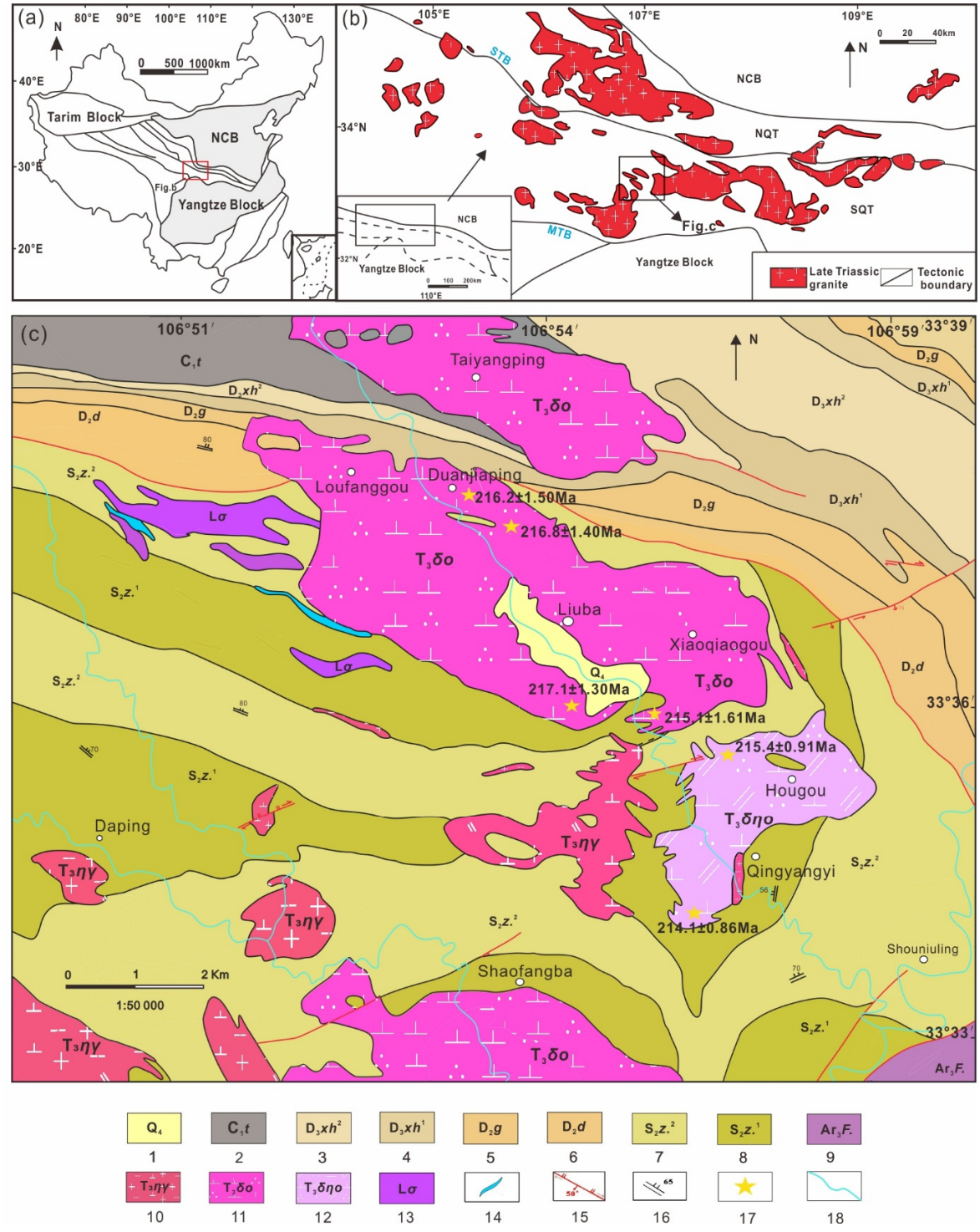


Figure 1. (**a**) Geotectonic sketch map of China [27]. (**b**) Distribution of Triassic granites in the Qinling Mountains [19], NCB: North China Block. NQT: North Qinling tectonic belt. SQT: South Qinling tectonic belt. MTB: Mianlue tectonic belt. STB: Shangdan tectonic belt. (**c**) Geological map showing distribution of the Liuba and Qingyangyi plutons in the South Qinling [15]. 1. Quaternary Holocene Series. 2. Tieshan Formation. 3. Upper rock member of Xinghongpu Formation. 4. Lower rock member of Xinghongpu Formation. 5. Gudaoling Formation. 6. Dafenggou Formation. 7. Upper member of Zhouqu Formation. 8. Lower member of Zhouqu Formation. 9. Foping Group. 10. Light gray fine-grained biotite granodiorite. 11. Light gray medium coarse quartz diorite. 12. Gray fine quartz monzodiorite. 13. Gray-green serpentinized peridotite. 14. Diorite dikes. 15. Brittle translational reverse fault and its occurrence. 16. Occurrence of deformation foliation. 17. Sampling location. 18. Rivers.

The main emerging stratigraphic units in the Liuba area include the Neoarchean–Palaeoproterozoic Foping Group, Silurian Bailongjiang Group, Devonian system, Carboniferous system, Permian system and Triassic system. The Palaeoproterozoic Fuping Group is a set of middle-to-high-grade metamorphic rock series; the main rock types are biotite plagioclase gneiss, marble and quartzite. The lower member of the Zhouqu Formation, Bailongjiang Group (Silurian) consists of meta-sandstone and -slate, meta-granule sandstone and siltstone and carbonaceous slate. The upper member includes carbonaceous slate, carbonaceous schist, silty slate, carbonaceous phyllite and meta-siltstone. The Lower Devonian Xichahe Formation is a set of conglomerate, sandstone and mudstone sedimentary assemblages; the Middle Devonian Shijiahe Formation is a sandstone, siltstone with limestone and calcareous slate sedimentary assemblage; the Middle Devonian Dafenggou Formation is a calcareous phyllite with calcareous silty phyllite; and the Middle Devonian Gudaoling Formation is a medium-thick bedded biogenic limestone, locally intercalated with quartz sandstone. The Upper Devonian Xinghongpu Formation consists of siltstone and calcareous siltstone. The Devonian system is generally characterized by coastal to shallow marine carbonate platform sedimentation. The Lower Carboniferous Tieshan Formation is primarily composed of a sedimentary assemblage of shallow marine sandy limestone, muddy limestone and limestone interbedded with minor silty slate. The Upper Carboniferous Sixiakou Formation is mainly composed of carbonaceous and siliceous slates. The Permian (Yangshan and Shuixiakou) Formation is mainly composed of thick-bedded limestone, thin-bedded limestone and mudstone limestone, while the Lower Triassic Liufengguan Formation is mainly composed of rhythmic layers of siltstone, calcareous slate and thin-bedded limestone. The fault structures in region are mainly near the east–west and NEE trending faults, and the scale of the near-east–west faults is larger.

3. Petrological Characteristics

3.1. Liuba Pluton

The long axis of the pluton in Liuba is NWW-oriented, with a width of 3~4 km, a length of 7~8 km, and an outlying area of about 30 km^2. The main lithology of the Liuba pluton is medium coarse-grained gray to light grey-green quartz diorite (Figure 2a). The weathered surface of the rock is gray, the fresh surface is light gray-green, with a medium coarse-grained granite texture and massive structure, and the mineral particle size is 0.5~2.5 mm (Figure 2b). The main mineral composition consists of plagioclase (52%~63%), quartz (5%~8%), alkaline feldspar (4%~7%), hornblende (10%~15%), and biotite (~8%), and the accessory minerals include zircon, apatite, titanite, and so on. Under the microscope, the alteration of plagioclase is obvious (Figure 2c), and it is subhedral lamellar, with a particle size of 0.5~2.0 mm. The quartz is heteromorphic granular with a particle size of 0.5~1.0 mm, mainly distributed in an interstitial pattern between feldspar grains, with wavy extinction. Most of the hornblende is transformed into biotite, the particle size is 0.5~1.0 mm, and it is green with obvious polychromism. Biotite has commonly undergone chloritization. The plagioclase in sample LB008 is obviously sericitized.

The Liuba pluton features well-developed MMEs with different sizes. The main body of the long axis is between 5 and 30 cm, predominantly oval-shaped. The lithology is mainly fine-grained monzodiorite and fine-grained quartz monzodiorite. MMEs exhibit a wide range of colors and particle sizes, and the colors are generally between light gray and gray black, which are obviously darker than the host rock (Figure 2d). MMEs are clustered and distributed; most of them have fine-grained texture. The main mineral composition of MMEs consists of plagioclase (45%~55%), alkaline feldspar (10%~15%), quartz (5%), hornblende (14%~18%), and biotite (10%~15%) (Figure 2e). The boundaries between the MMEs and the host rock are mostly in complete contact, and the condensation

edge phenomenon can be clearly seen in some MMEs. The size of MMEs is 5~60 cm, the smallest being only 1~3 cm. The apatites in the host rock of the Liuba pluton are short columns with a ratio of 3:1~8:1. The apatites in the MMEs are acicular or long-columnar, and the length-to-width ratio is 10:1~30:1 (Figure 2f,i).

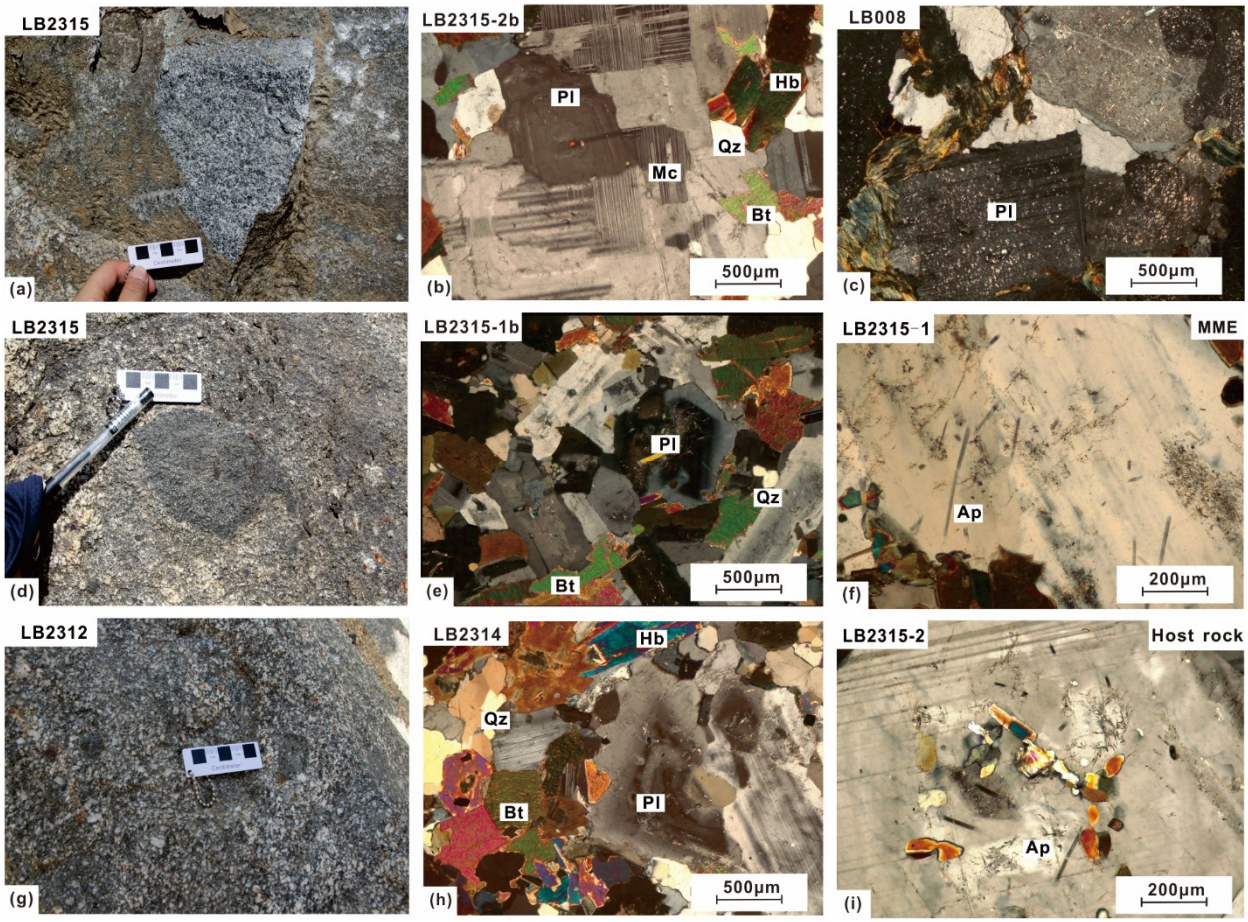


Figure 2. Representative field photographs and photomicrographs of the Liuba and Qingyangyi plutons. (**a**) Quartz diorite of Liuba pluton; (**b**) photomicrograph of quartz diorite; (**c**) plagioclase sericite; (**d**) MME of Liuba pluton; (**e**) photomicrograph of MME; (**f**,**i**) photomicrographs of apatite; (**g**) quartz monzodiorite of Qingyangyi pluton; (**h**) photomicrograph of quartz monzodiorite. Mineral abbreviations: Pl—plagioclase feldspar; Hb—hornblende; Qz—quartz; Mc—microcline; Bt—biotite; Ap-apatite.

3.2. Qingyangyi Pluton

The long axis of the Qingyangyi pluton is distributed in a NE direction, about 3~4 km wide and 3~4 km long, and has an exposed area of about 14 km^2. The main lithology of the Qingyangyi pluton is medium coarse gray–light gray quartz monzodiorite (Figure 2g). The main mineral components are plagioclase (50%~55%), quartz (5%~10%), alkaline feldspar (10%~15%), hornblende (10%~15%), and biotite (5%~10%), and the accessory minerals are zircon, apatite, sphene, and magnetite. The plagioclase is irregularly subhedral lamellar–heteromorphic, with the development of polycrystalline twinning and a zonation texture with a grain size of 0.5~6 mm. The quartz is heteromorphically granular with a particle size of 0.1~0.5 mm. It is mainly interstitial distributed among feldspar grains with wavy extinction. The microcline exhibits a distinct lattice twin crystal and striped texture, with mineral crystals displaying a granular texture, and the grain size ranges from 1.5 to 2.5 mm (Figure 2h). MMEs are occasionally seen in the rock.

4. Analytical Methods

4.1. Whole-Rock Geochemical Analyses

A total of 15 whole-rock geochemical samples (LB007–LB010, LB2312–LB2315) and 6 isotopic chronology samples (LB007, LB008, LB009, LB010, LB2312, LB2315) from diorite rocks were collected for analysis. The major elements, trace elements, and rare earth elements of the 15 whole-rock geochemical samples were analyzed. These analyses were conducted at Wuhan Sample Solution Technology Co., Ltd. (Wuhan, China). Prior to testing, the samples were ground to a 200 mesh powder. The major elements were then determined using a wavelength-dispersive X-ray fluorescence spectrometer, which was manufactured by Rigaku Corporation, based in Tokyo, Japan. The X-ray fluorescence spectral analysis fusion method was in accordance with national standard GB/T14506.28-2010 [28], with a relative error of less than 2%. Trace elements were determined using an Agilent 7700e inductively coupled plasma mass spectrometer, which was manufactured by Agilent Technologies, based in Santa Clara, CA, USA. with a relative error of less than 5%. Refer to Chen et al. 2000 for the test process of chemical analysis [27].

4.2. LA-ICP-MS Zircon U-Pb Dating

The crushing of isotope dating samples, zircon separation, selection and target making, zircon dating samples, and zircon cathodoluminescence photography of dating samples were completed by Wuhan Sample Solution Technology Co., Ltd. Zircon dating was performed using the Agilent inductively coupled Plasma Mass Spectrometer (Agilent 7900), is manufactured by Agilent Technologies, based in Santa Clara, CA, USA. and the coherent 193 nm excimer Laser denudation System (GeoLas HD) using the LA-ICP-MS method. When dating the sample zircon, the cathodoluminescence (CL) images and the transmitted light transmission image of the zircon were combined first to avoid the cracks on the surface of the zircon and select the dating crystal domain. A 193 nm laser was used to denude the zircon. The diameter of the spot beam for laser denudation was 32 μm. The standard sample for trace element correction was NIST 610, the standard sample for isotope ratio correction was 91,500, and the recognized reference age of the standard sample was 1062 ± 10 Ma [29]. The content of the GJ-1 and GJ-2 elements was calculated using silicate glass NISTRM610 synthesized by the US National Bureau of Standard Materials as the external standard, and ^{29}Si was used as the inner table element for correction; the recognized reference age of the standard sample was 599 ± 6 Ma [29]. The experimental data were processed using the ICPMSDataCal 10.8 program and Isoplot 4.15 program, and the common lead was corrected by the ^{208}Pb correction method [30]. The recommended element content values for NIST glass were sourced from the GeoReM database http://georem.mpch-mainz.gwdg.de (accessed on 8 January 2023). Detailed analytical procedures are described by Liu [31,32].

5. Results

Whole-rock geochemical and zircon U-Pb age analysis results of Liuba and Qingyangyi plutons are shown in Supplementary Tables S1 and S2.

5.1. Whole-Rock Major and Trace Elements

The Liuba pluton quartz diorite is more acidic than the MMEs, with higher SiO_2 and Na_2O contents. In the QAP diagram (Figure 3a), the host rock samples fall into the quartz diorite field. In the TAS diagram (Figure 3b), the samples fall into the sub-alkaline granodiorite field. The quartz diorite samples of Liuba pluton contain SiO_2 (66.10~69.43 wt.%) and Na_2O/K_2O (1.26~2.65), which are relatively rich in Na. The content of other compounds is as follows: Al_2O_3 was high; ranging from (15.35~16.55 wt.%); MgO (0.98~2.21 wt.%); TFe_2O_3 (2.54~3.31 wt.%); TiO_2 (0.38~0.45 wt.%); P_2O_5 (0.09~0.12 wt.%);

and CaO (1.51~4.36 wt.%) (Supplementary Table S1). Mg# values range from 46.45 to 61.28, which are lower than the primitive magma (Mg# > 70), suggesting that these magmas have undergone a relatively intense crystal fractionation. In the K_2O-SiO_2 diagram (Figure 3c), most of the quartz diorite samples of the Liuba pluton fall with in the field of the high-K calc-alkaline series.

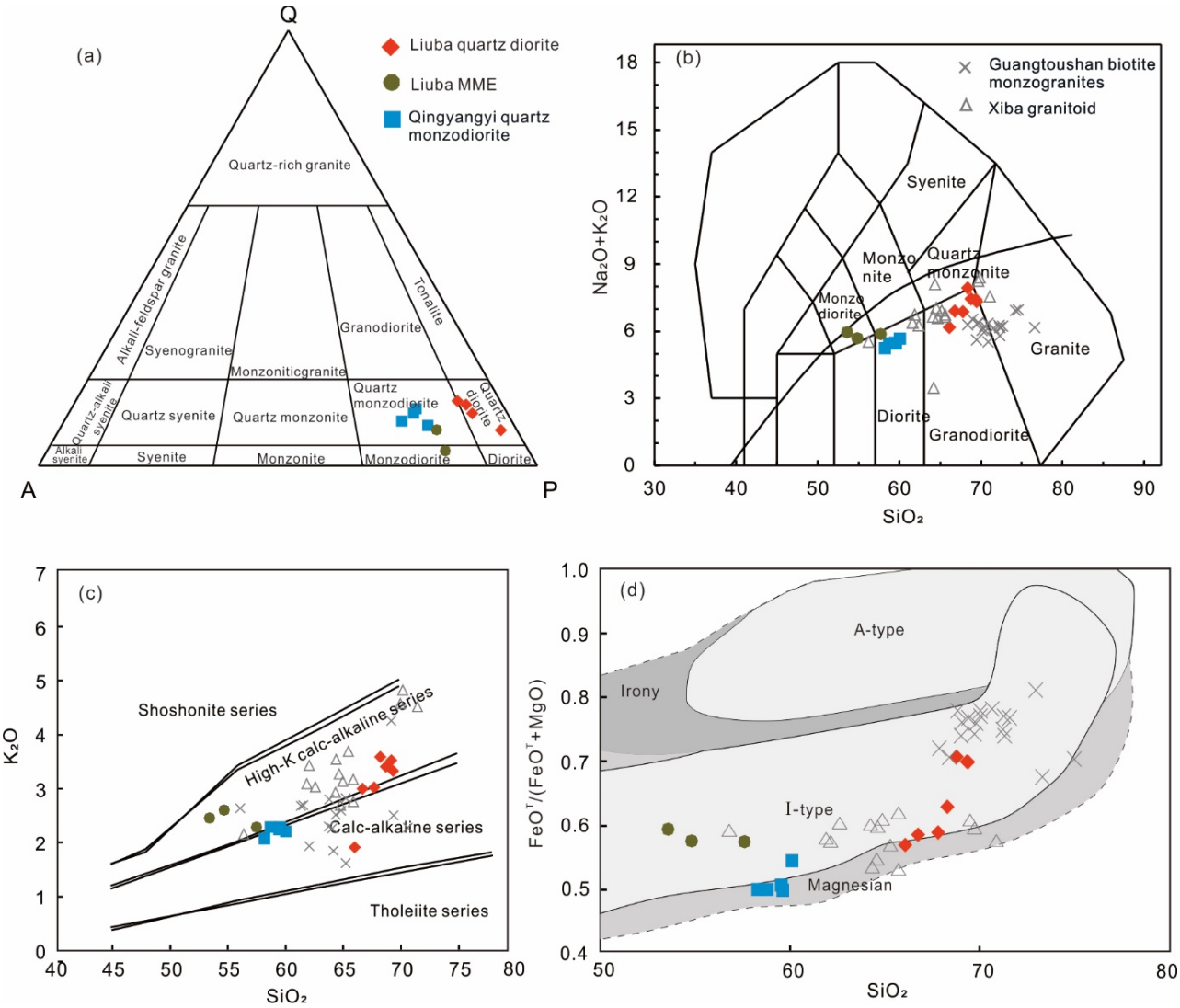


Figure 3. (**a**) QAP diagrams [33] (**b**) TAS diagrams [34] (**c**) K_2O vs. SiO_2 diagrams [35] (**d**) $FeO^T/(FeO^T + MgO)$ vs. SiO_2 diagrams [36] for Liuba quartz diorite, MMEs and Qingyangyi quartz monzodiorite. The data from the Guangtoushan and Xiba plutons are from Guan et al. and Liu et al. [37,38].

The MME samples (LB2315-1) from the Liuba pluton have a SiO_2 content of 57.61 wt.%. In the QAP diagram (Figure 3a), the sample falls within the quartz monzodiorite field. In the TAS diagram (Figure 3b), they are located in the subalkaline diorite field. The Na_2O/K_2O ratio is 1.86, indicating a relative enrichment in Na. The Al_2O_3 content is relatively high at 17.46 wt.%, with MgO at 4.26 wt.%, total Fe_2O_3 at 6.39 wt.%, TiO_2 at 0.81 wt.%, P_2O_5 at 0.23 wt.%, and CaO at 6.16 wt.%. The Mg# value is 60.84. In the SiO_2-K_2O diagram (Figure 3c), the sample falls within the high-K calc-alkaline series field. The MME samples (2315-3, 2315-4) of the Liuba pluton have a SiO_2 content of 53.50~54.81 wt.%. In the QAP diagram and TAS diagram (Figure 3a,b), the samples all fall into the field of monzodiorite. The value of Na_2O/K_2O was 1.39~1.68, which was relatively rich in

Na. The contents of Al_2O_3, MgO, TFe_2O_3, TiO_2, P_2O_5 and CaO is (16.80~17.78 wt.%), (4.84~5.03 wt.%), (7.59~7.87 wt.%), (0.95~1.06 wt.%), (0.28~0.36 wt.%) and (6.94~7.09 wt.%) respectively. Mg# values ranges from 58.91 to 60.67. In the SiO_2-K_2O diagram (Figure 3c), the samples fall in the field of the high-K calc-alkaline series (Supplementary Table S1).

The Qingyangyi quartz monzodiorite samples exhibit a content of SiO_2 (58.29~ 60.14 wt.%). In the QAP diagram (Figure 3a), the samples fall within the quartz monzodiorite field. In the TAS diagram (Figure 3b), the samples are situated in the subalkaline diorite field. The Na_2O/K_2O ratio ranges from 1.63 to 1.85, indicating a relative enrichment in Na. The Al_2O_3 content is relatively high (15.44~16.18 wt.%), while MgO is (4.40~5.92 wt.%), TFe_2O_3 (5.85~6.58 wt.%), TiO_2 (0.64~0.69 wt.%), P_2O_5 (0.18~0.21 wt.%), CaO (5.66~6.29 wt.%), and Mg# (63.66~67.79). In the K_2O-SiO_2 diagram (Figure 3c), the samples fall into the high-K calc-alkaline series field (Supplementary Table S1).

The characteristics of trace elements and rare earth elements (REE) in the Liuba and Qingyangyi plutons are similar. The chondrite-normalized REE pattern diagrams of the two plutons both show strong light and heavy rare earth element fractionation, with a generally rightward inclination. The heavy rare earth element (HREE) partition pattern is flat, showing a weak negative Eu* anomaly (Figure 4a). All rocks types are enriched in light rare earth elements (LREE) and depleted in HREE. The REE content of the Liuba MMEs from the pluton is higher than that of the Liuba quartz diorite and the Qingyangyi quartz monzodiorite. Among them, the light and heavy rare earth element (LREE/HREE) fractionation of the (LB2315-1) quartz monzodiorite is greater than that of the Liuba quartz diorite and the Qingyangyi quartz monzodiorite. In contrast, the LREE/HREE fractionation of the (LB2315-3, LB2315-4) monzodiorites is less than that of the Liuba quartz diorite and the Qingyangyi quartz monzodiorite. The primitive mantle-normalized trace element spider diagrams show enrichment in large-ion lithophile elements (LILE) such as Rb, Ba, and K, and relative depletion in high-field strength elements (HFSE) such as Nb, Ti, Ba, and P. The primitive mantle-normalized trace element spider diagrams of MMEs closely resemble those of host rock (Figure 4b) (Supplementary Table S1).

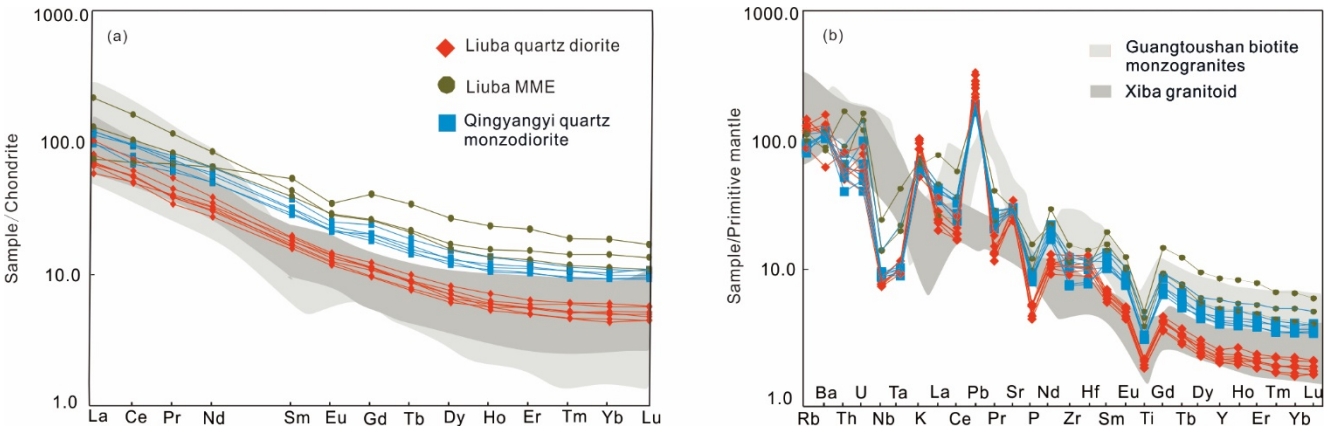


Figure 4. (**a**) Chondrite-normalized REE patterns and (**b**) primitive mantle-normalized trace element spider diagrams of Liuba quartz diorite, MMEs, and Qingyangyi quartz monzodiorite [39]. The chondrite and primitive mantle values are from Sun and McDonough (1989), respectively [40].

The total content of REE in Liuba pluton quartz diorite was (72.7~110) ppm, with an average of 86.1 ppm. The fractional of LREE and HREE is obvious, with LREE/HREE values of 8.95~14.0. The Eu* anomaly is (0.92~0.98) ppm, indicating a weak overall negative Eu anomaly (Figure 4a,b). The internal differentiation of LREE is obvious, with $(La/Sm)_N$ values of (3.28~4.35) (mean value 4.05), La/Yb values (16.1~29.1) (mean value 21.2), and

$(La/Yb)_N$ values of (10.8~19.6) (mean value 10.7) and a $(Gd/Yb)_N$ value of (2.01~2.26) (mean value is 2.14) (Supplementary Table S1).

The total content of REE in the Liuba pluton quartz dioritic MMEs (2315-1) is higher than that of the host rock, and the total REE content is 247 ppm. LREE/HREE value is 14.0, and the degree of differentiation is lower than that of host rock. Generally, the negative Eu* (Eu* = 0.84) anomaly is weak. The internal differentiation of LREE is obvious, with a $(La/Sm)_N$ value of 4.94, La/Yb value of 28.58, $(La/Yb)_N$ value of 19.3, and (Gd/Yb) value of 2.31 (Figure 4a,b). The total REE content in Liuba pluton diorite MMEs (2315-3, 2315-4) is also higher than that of the host rock, ranges from (143 to 170) ppm, with an average of 157 ppm. There is a notable fractionation between LREE and HREE, with a ratio ranges from 4.16 to 8.37, indicating a lesser degree of differentiation than the host rock. The Eu* anomaly is (0.73~0.90), suggesting a weak negative Eu anomaly overall. The internal differentiation of LREE is obvious, with $(La/Sm)_N$ values of (1.31~3.23) (mean value 2.27) and La/Yb values of (5.65~13.32) (mean value 9.48), of $(La/Yb)_N$ values (3.81~8.98) (mean value 6.39), and of $(Gd/Yb)_N$ values (2.29~2.74) (mean value 2.51) (Figure 4a,b) (Supplementary Table S1).

The total REE content in Qingyangyi pluton quartz monzodiorite is (119~156) ppm, with an average of 140 ppm. The fractionation of LREE and HREE is obvious, and the LREE/HREE values are 8.57~10.1. The Eu* anomaly is (0.83~0.95). Generally, the negative Eu anomaly is weak. The internal differentiation of LREE is obvious, with $(La/Sm)_N$ values of (2.92~3.72) (mean value 3.38), La/Yb values of (15.0~18.0) (mean value 16.1), $(La/Yb)_N$ values of (10.1~12.2) (mean value 10.9), and $(Gd/Yb)_N$ values of (1.93~2.20) (mean value 2.05) (Figure 4a,b) (Supplementary Table S1).

5.2. Zircon U-Pb Age

5.2.1. Zircon U-Pb Ages of Quartz Diorite in Liuba Pluton

The quartz diorite age sample (LB007) of the Liuba pluton was taken from Duanjiaping in the northern part of the pluton (N 33°37′45″, E 106°53′20″) (Figure 1c). The zircons are mostly idiomorphic crystals with a particle size of about 80–150 μm and an aspect ratio of 1:1~3:1. The CL images of the zircon shows that the growth belt of the zircon is obvious (Figure 5). The Th/U ratios are (0.13~0.98), all of which are greater than 0.1 (Supplementary Table S2) (Figure 6a). Of the 24 analyzed zircons, 23 grains were analyzed on or near the U–Pb concordance lines (concordance > 90%). Moreover, the zircons showed relative enrichment in HREE and relative depletion in LREE. The chondrite-normalized REE patterns with significant negative Eu* anomaly and positive Ce anomaly (Figure 6b, Supplementary Table S2), combined with the zircon lithography characteristics, suggesting a magmatic origin [41–43]. The ^{207}Pb-^{206}Pb ages of measuring points 3 and 11 are 1231 ± 48 Ma and 981 ± 48 Ma, respectively, which may represent the ages of xenocryst zircons. Among them, the ^{206}Pb-^{238}U ages at 7 test points are relatively concentrated, with a weighted mean age of 216.2 ± 1.5 Ma (MSWD = 0.75) (Figure 7a).

The quartz diorite age sample (LB008) of the Liuba pluton was taken from the pluton north of Liuba (N 33°37′20″, E 106°53′44″) (Figure 1c). The zircons are mostly idiomorphic crystals with a particle size of about 80 to 150 μm and an aspect ratio of 1:1~3:1. The zircon particles are more idiomorphic short columns, and the CL images of the zircons show obvious growth zoning (Figure 5). The Th/U ratios (0.14~0.37), all of which are greater than 0.1, suggest a magmatic origin (Supplementary Table S2) (Figure 6a,b). Of the 24 analyzed zircons, 21 grains were analyzed on or near the U–Pb concordance lines (concordance > 90%) (Figure 7b). Among them, the ^{206}Pb-^{238}U ages at 19 test points are relatively concentrated, with a weighted mean age of 216.1 ± 0.8 Ma (MSWD = 0.67) (Figure 7b).

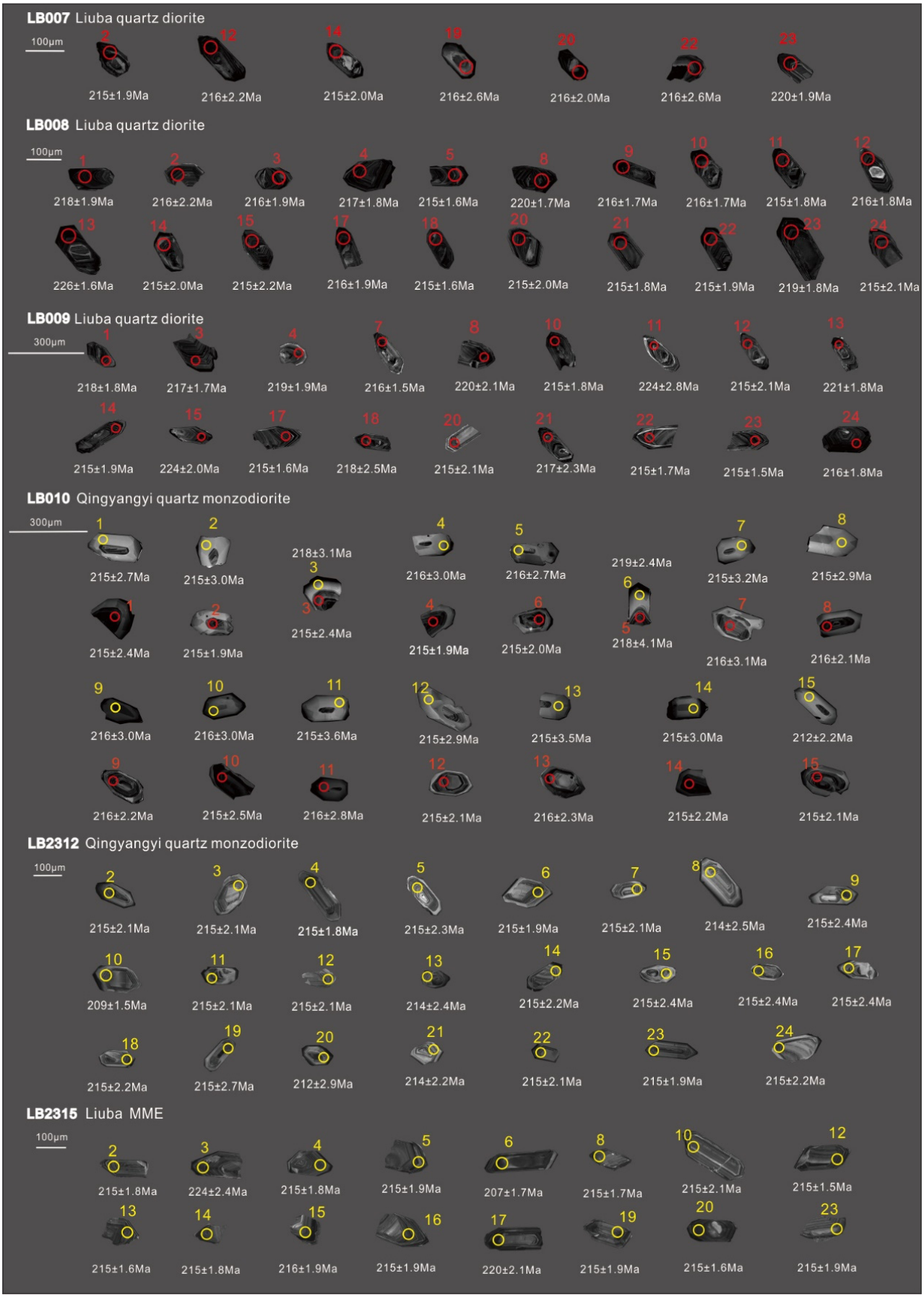


Figure 5. Cathodoluminescence (CL) images and zircon U-Pb ages from Liuba and Qingyangyi plutons.

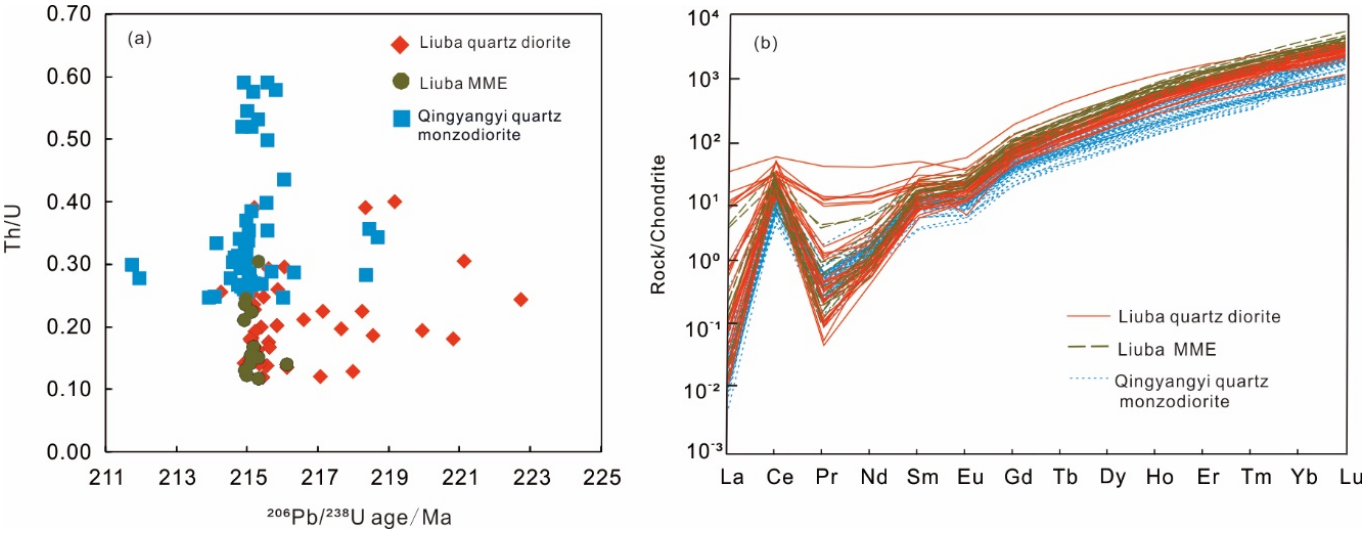


Figure 6. (**a**) Zircons Th/U vs. $^{206}Pb/^{238}U$ age and (**b**) chondrite−normalized REE Pattern of zircons [41]. The chondrite-normalized values based on Corfu F (2003).

The quartz diorite age sample (LB009) of the Liuba pluton was taken from the southern pluton of Liuba (N 33°36′40″, E 106°54′58″) (Figure 1c). The zircons are mostly idiomorphic crystals with a particle size of about 100~200 μm and an aspect ratio of 1:1~4:1. The zircon particles are more idiomorphic and short-columnar, and the CL images of the zircons show obvious growth zoning (Figure 5). The Th/U ratios (0.11~0.28), all of which are greater than 0.1, suggest a magmatic origin (Supplementary Table S2) (Figure 6a,b). Of the 24 analyzed zircons, 21 grains were analyzed on or near the U–Pb concordance lines (concordance > 90%). Among them, the ^{206}Pb-^{238}U ages at 18 test points are relatively concentrated, with a weighted mean age of 217.1 ± 1.3 Ma (MSWD = 2.00) (Figure 7c).

The Liuba pluton diorite MME age sample (LB2315) was taken from near the entrance highway on the southern side of the Liuba pluton (N 33°36′26″, E 106°56′20″) (Figure 1c). The zircons are mostly idiomorphic crystals with a particle size of (80~200) μm and an aspect ratio of 1:1~4:1. The zircon particles are more idiomorphic short columns, and the CL images of the zircons show obvious growth zoning (Figure 5). Of the 24 analyzed zircons, 22 grains were analyzed on or near the U–Pb concordance lines (concordance > 90%). Among the zircons measured, only one has a Th/U ratio < 0.1, and the others range from 0.06 to 0.55, indicating a magmatic origin (Supplementary Table S2) (Figure 6a,b), in which the ^{206}Pb-^{238}U ages of test points 11, 9, 18, 21, and 7 are 1010 ± 7 Ma, 969 ± 7 Ma, 928 ± 11 Ma, 917 ± 5 Ma and 547 ± 8 Ma, respectively, which may represent the ages of xenocryst zircons. The age of ^{206}Pb-^{238}U at 14 points is concentrated, with a weighted mean age of 215.4 ± 1.0 Ma (MSWD = 0.39) (Figure 7d).

In summary, the crystallization ages of quartz diorite and dioritic MMEs in Liuba pluton are very similar, ranging from 215 to 217 Ma, both of which are products of late Triassic magmatism.

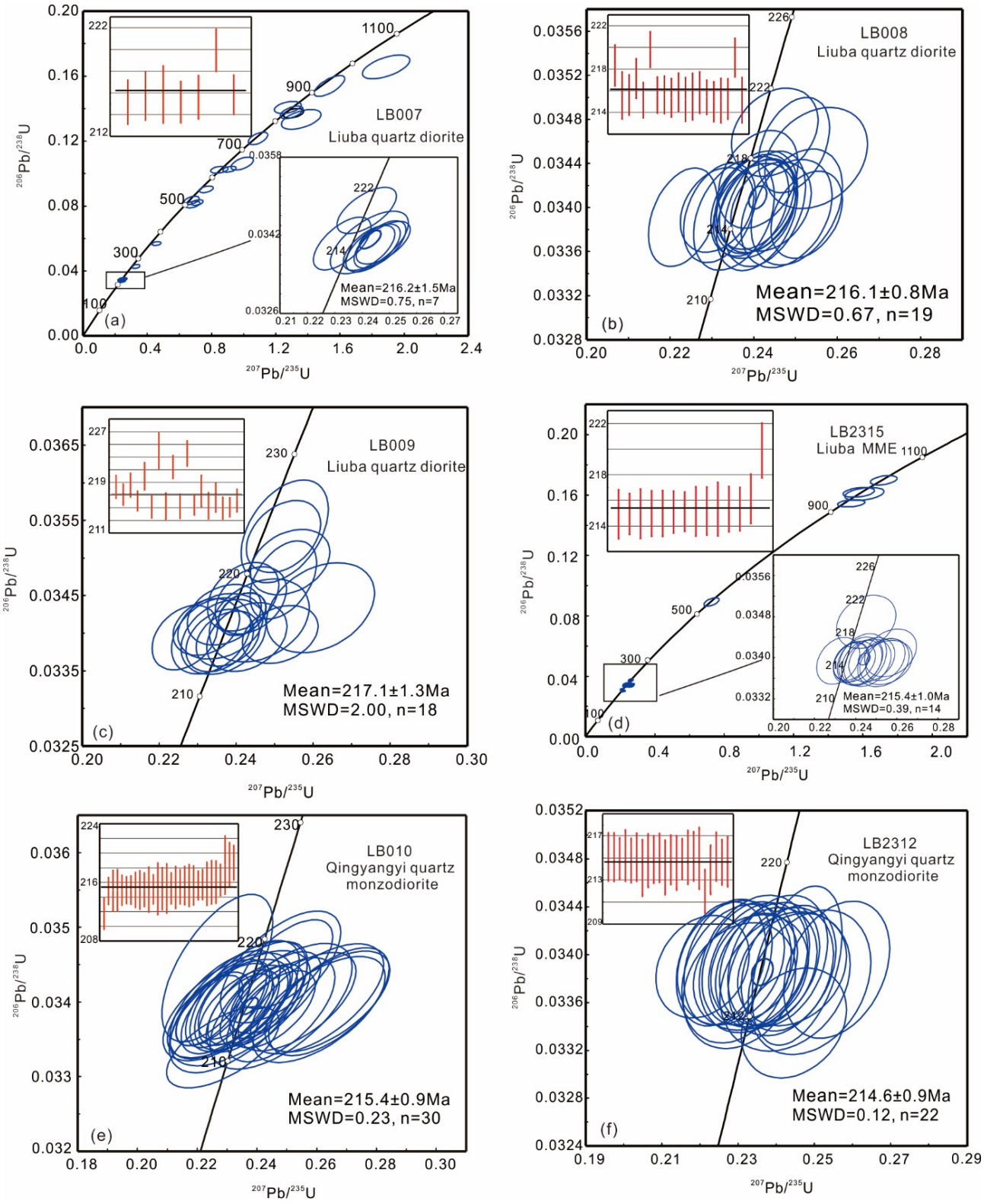


Figure 7. LA-ICP-MS zircon U-Pb concordance diagrams of Liuba quartz diorite, MMEs, and Qingyangyi quartz monzodiorite. (**a**) U-Pb concordia diagrams and $^{206}Pb/^{238}U$ weighted mean ages of LB007 sample; (**b**) U-Pb concordia diagrams and $^{206}Pb/^{238}U$ weighted mean ages of LB008 sample; (**c**) U-Pb concordia diagrams and $^{206}Pb/^{238}U$ weighted mean ages of LB009 sample; (**d**) U-Pb concordia diagrams and $^{206}Pb/^{238}U$ weighted mean ages of LB2315 sample; (**e**) U-Pb concordia diagrams and $^{206}Pb/^{238}U$ weighted mean ages of LB010 sample; (**f**) U-Pb concordia diagrams and $^{206}Pb/^{238}U$ weighted mean ages of LB2312 sample.

5.2.2. Zircon U-Pb Ages of Quartz Monzoniorite in the Qingyangyi Pluton

The quartz monzodiorite age sample (LB010) from the Qingyangyi pluton was taken from the North Qingyangyi Village Qingyangyi pluton (N 33°35′26″, E 106°56′30″) (Figure 1c). The zircons are mostly idiomorphic crystals with a particle size of (80~250) μm and an aspect ratio of 1:1~3:1. The zircon particles are more idiomorphic short columns, and CL images of the zircons (Figure 5) show that some zircon growth bands are not obvious. A total of 28 zircons were analyzed at 30 points (Supplementary Table S2). The Th/U ratio (0.24~0.55), all of which are greater than 0.1, indicate these zircons are magmatic zircons (Figure 6a,b). All 24 measuring points are valid analysis points (Figure 7e), and the ^{206}Pb-^{238}U ages at 30 measuring points are concentrated. The weighted mean age is 215.4 ± 0.9 Ma (MSWD = 0.23) (Figure 7e).

The quartz monzodiorite age sample (LB2312) from the Qingyangyi pluton was taken from the Xianggou Qingyangyi pluton (N 33°34′40″, E 106°56′58″) (Figure 1c). The zircons are mostly idiomorphic crystals with a particle size of (50~200) μm and an aspect ratio between 1:1 and 3:1. The zircon particles are more idiomorphic short columnar and rounded, and the CL images of the zircon show obvious growth zoning (Figure 5). Of the 24 analyzed zircons, 23 grains were analyzed on or near the U–Pb concordance lines (concordance > 90%) (Figure 7f). The Th/U ratios (0.24~0.32), all of which were greater than 0.1, suggest a magmatic origin (Supplementary Table S2) (Figure 6a,b). The ^{206}Pb-^{238}U ages of the 22 test points are concentrated, with a weighted mean age of 214.6 ± 0.9 Ma (MSWD = 0.12) (Figure 7f).

6. Discussion

6.1. The Formation Age of Diorite

Six representative samples from the Liuba and Qingyangyi plutons were chosen for zircon U–Pb dating, with detailed LA-ICP-MS zircon U–Pb dating data listed in Supplementary Table S2.

Three samples (LB007, LB008, LB009) were selected from the Liuba pluton quartz diorites. The weighted mean ^{206}Pb-^{238}U ages of zircons are 216.2 ± 1.5 Ma (MSWD = 0.75, n = 7), 216.1 ± 0.8 Ma (MSWD = 0.67, n = 19), and 217.1 ± 1.3 Ma (MSWD = 2.00, n = 18), respectively (Figure 7a–c). One sample (LB2315) was selected from the Liuba pluton dioritic MMEs (Figure 7d). The weighted mean ^{206}Pb-^{238}U ages of zircons are 215.4 ± 1.0 Ma (MSWD = 0.39, n = 14). Two samples (LB010, LB2312) were obtained from the Qingyangyi quartz monzodiorite. Both yielded a weighted mean ^{206}Pb-^{238}U age of 215.4 ± 0.9 Ma (MSWD = 0.23, n = 30) and 214.6 ± 0.9 Ma (MSWD = 0.12, n = 22), respectively (Figure 7e,f). The ages of these samples are basically consistent within the margin of error, which indicates that the crystallization ages of the Qingyangyi quartz monzodiorite and Liuba quartz diorite are in the late Triassic of the early Mesozoic, and the MMEs formed at the same time as the host rock.

6.2. Magmatic Evolution and Petrogenesis

6.2.1. The Liuba and Qingyangyi Plutons

The two late Triassic intermediate-acid intrusive pluton in the South Qinling are mainly quartz diorite and quartz monzodiorite, belonging to the high-K calc-alkaline series. The main element is Na (Na_2O/K_2O value is 5.23~6.17), the aluminum saturation index A/CNK is between 0.82~1.10, with an average of 0.92, and the Mg# values range from 58.9 to 67.7. In addition, with the increase in SiO_2 content, the contents of P_2O_5 and CaO gradually decrease, which is significantly different from the evolution trend of S-type granite, and the depletion of Nb, P and Ti also shows the characteristics of I-type granite [9].

Moreover, in the $FeO^T/(FeO^T + MgO)$-SiO_2 diagram (Figure 3d), it is indicated that Liuba quartz diorite and Qingyangyi quartz monzodiorite belong to the category of I-type granite.

Zircon U-Pb dating shows that the Liuba pluton has zircon ages of 981 Ma and 1231 Ma, indicating the presence of xenocryst zircon from ancient rock strata and suggesting that the magma source area is mainly composed of relatively complex ancient crustal materials. The SiO_2 content of Liuba pluton quartz diorite and Qingyangyi pluton quartz monzodiorite is higher than that of the lower crust, the contents of Al_2O_3, K_2O and Na_2O are equivalent to or slightly higher than those of the lower crust, the contents of Fe_2O_3 and MgO are lower than those of the lower crust, and the compatibility elements Cr and Ni have extremely low contents, significantly lower than those in the lower crust. According to the preliminary analysis of major elements and trace elements, the quartz diorite and quartz monzodiorite could not have been directly formed by partial melting of the mantle, but may have been formed by partial melting of the lower crust rocks [44]. The Nb/Ta values (9.87~17.34, average of 13.79) of the quartz monzodiorite and quartz diorite, which is close to the crustal Nb/Ta value (11–14), excluding a single source from the lower crust and possibly the addition of mantle materials [45–49]. Ta/U values (0.20~0.50, average of 0.34), Nb/U values (2.70~7.30, average of 4.73), all of which are far smaller than the MORB/OIB values (Ta/U~2.7, Nb/U~47) [50]. It is closer to the crust (Ta/U~1.1, Nb/U~12.1), suggesting a crustal source [44]. The strong depletion of Ti, Nb, and Ta further supports the idea that the magma's source is primarily crustal. The Y/Yb values (10.28~11.88) are close to 10, indicating that hornblende is the dominant residual phase in the source [51]. In the magmatic source region identification diagram (Figure 8a,b), the samples generally fall in the partial melting zone of basic rocks, indicating that the parent magma mostly originated from the partial melting of the lower crust. This is consistent with the conclusion that the surrounding plutons (the Guangtoushan and Xiba plutons) are primarily derived from the partial melting of the crust during the formation process [37].

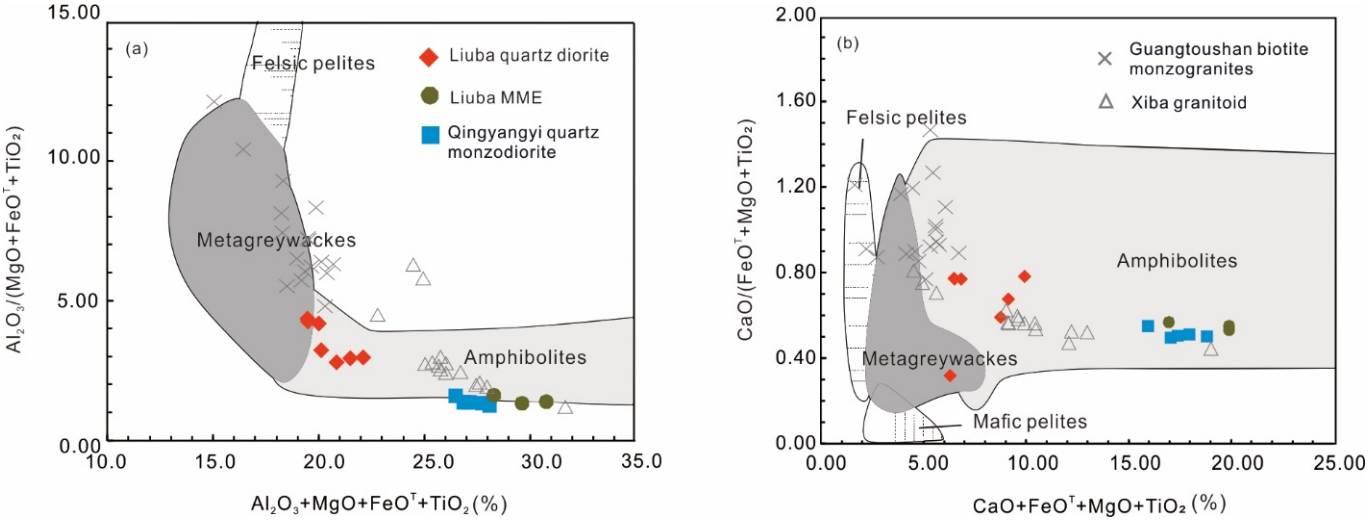


Figure 8. Discrimination diagrams of source compositions: (**a**) $Al_2O_3/(MgO + FeO^T + TiO_2)$ vs. $Al_2O_3 + MgO + FeO^T + TiO_2$ (**b**) $CaO/(FeO^T + MgO + TiO_2)$ vs. $CaO + FeO^T + MgO + TiO_2$ of Liuba quartz diorite, MMEs, and Qingyangyi quartz monzodiorite [45,46].

Compared to the Cr (500~600 ppm and Ni (500~600 ppm) contents derived from mantle peridotite [52], the Cr content (5.63~68.8) ppm and Ni (2.83~22.2) ppm in the quartz diorite of the Liuba pluton, Cr content (81.4~133.8) ppm and Ni (12.3~20.7) ppm in MMEs, the Cr content of (150~272 ppm and Ni (43.8~94.9 ppm) in the quartz monzodiorite of the Qingyangyi pluton are all lower than the values from the mantle peridotite, indicating that

they have undergone certain degree of magmatic evolution. The Mg# value is an important index to judge the presence of mantle interaction. Experimental petrology indicates that the average Mg# value are 53.8 for the quartz diorite in the Liuba pluton, 60.1 for the MMEs, and 66.8 for the Qingyangyi pluton, all of which are lower than the range of primary magma Mg# values. This suggests that during the magmatic evolution process, there may have been a separation and crystallization of mafic minerals [48,52]. According to the Harker diagram, related to SiO_2 (Figure 9), P_2O_5, Fe_2O_3, CaO, TiO_2, and MgO have a good linear relationship with SiO_2, the total amount of REEs in different rocks of the same pluton has a large variation region, and the characteristics of REEs in the MMEs are also significantly different from those in the host rocks. This implies that there must be an incorporation of components with distinctly different REE characteristics into the Liuba pluton, and the host rock and the MMEs exhibit a good linear relationship, indicating the presence of magma mixing [53]. In Figure 10a, the samples all show characteristics of partial melting rather than crystalline separation.

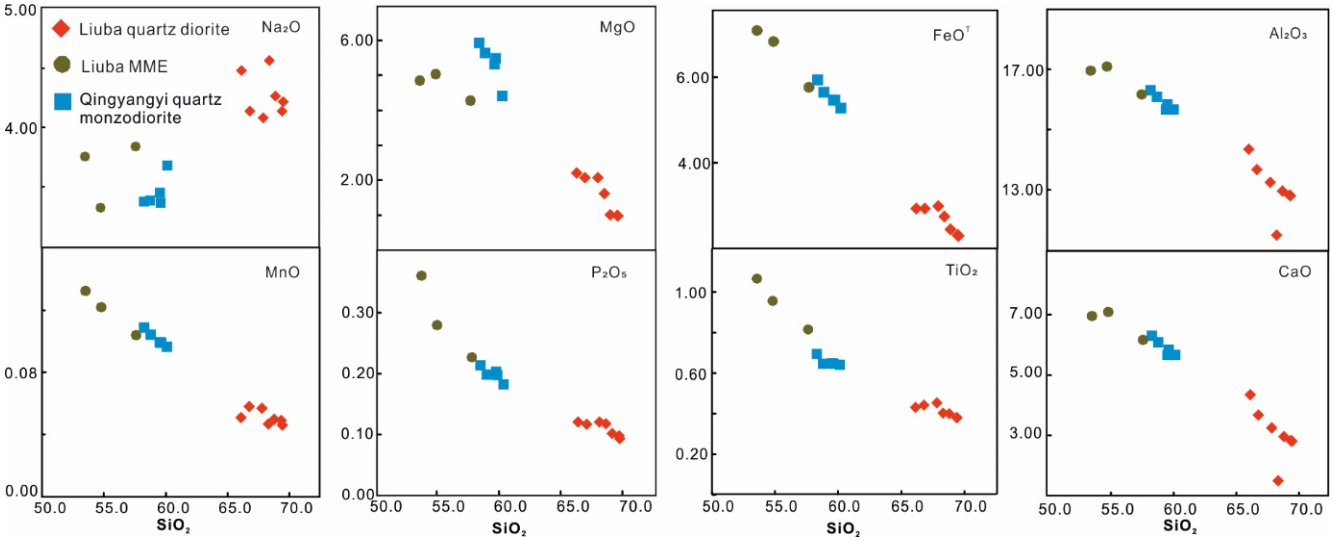


Figure 9. SiO_2 vs. major element oxides of Liuba quartz diorite, MMEs, and Qingyangyi quartz monzodiorite.

A large number of high-Sr- and low-Y-type granites were produced in the South Qinling in the early Mesozoic, in the Hejiazhuang granodiorite pluton (247 ± 4 Ma) from north to south, as well as Xiba pluton dioritic granite and granodiorite (about 219 Ma); Huahongshuping pluton granodiorite (214 ± 2.7 Ma); Guangtoushan pluton granodiorite (216 ± 2 Ma), Jiangjiaping pluton biotite granite (206 ± 2 Ma) [16,53–56]. These plutons, including the Liuba pluton and the Qingyangyi pluton, exhibit high-Sr and low-Y characteristics, indicating that they have been influenced by mantle-derived materials; except for the Hejiazhuang pluton, which shows a distinct positive Eu anomaly, the others generally present slight or negative Eu anomalies, and the formation age of these granitic pluton is concentrated at 219~200 Ma. This reflects the phenomenon of crust–mantle interactions caused by regional crustal thickening during the early Mesozoic in the South Qinling area and also indicates the widespread occurrence of granitoid rocks in either a spotty or planar distribution, which may be a material response to the lower crust material removal event in the later period of collision orogeny [53,57–63].

Under conditions of water undersaturation, the partial melting of basaltic magma can lead to the formation of sub-aluminous tonalitic to granodioritic magmas. Current experimental petrography indicates that only mature island arc high-K calc-alkaline basalt–andesite and andesite partial melting can produce high-K calc-alkaline granite [64], and

the Neoproterozoic basement rocks emerging in the South Qinling tectonic belt and the northern margin of the Yangtze Block are mainly basic volcanic rocks. The age of the isotope Nd is mostly concentrated around 1.1 Ga [65–72]; the whole-rock Nd model age of Triassic granites in the South Qinling tectonic belt is also concentrated around 1.1 Ga [61,73] and belongs to the late Mesoproterozoic, which indicates that these granites originated from the re-melting of the Proterozoic crust, so the source rocks of these granites may be the Neoproterozoic basement rocks distributed in the South Qinling tectonic belt and the northern margin of the Yangtze Block [72]. Therefore, the Liuba pluton and Qingyangyi pluton may also originate from the re-melting of the Proterozoic crust.

In summary, the Liuba and Qingyangyi plutons may originate from the partial melting of the Proterozoic lower crust.

6.2.2. Magmatic Mixing

At present, there are three main viewpoints on the origin of MMEs in magmatic rocks: (1) They are residual bodies from the melting source region of granite or xenoliths from the surrounding rock [74]. (2) The early cumulate minerals of the host rock are also referred to as co-genetic enclaves [75–77]. (3) They are the mixing result of the injection of mafic magma into felsic magma [78–80].

Liuba pluton quartz diorite is rich in MMEs which are elliptical in shape, with a clear boundary against the host rock. They exhibit the typical characteristics of magma enclaves in terms of petrology and mineralogy with no metamorphic texture or foliation structure, and the mineral particle size is significantly smaller than that of the host rock. Their mineral composition is similar to that of the host rock, but the content of magnesia–iron minerals is higher. The MMEs are rich in biotite and plagioclase, but lack deep-source metamorphic minerals, which rules out the possibility of their being refractory residues from the source region [81,82]. No zonation of thermal or contact metamorphic components was observed under solid-state conditions, indicating that MMEs are not part of the surrounding rock xenolith. Co-genetic enclaves are mainly formed at the margin of magma channel and early crystallizing dark minerals can rapidly cool and accumulate to form MMEs, which are concentrated at the margins of a pluton. However, field investigations have found that the number of MMEs increases and their size enlarges near the center of the Liuba pluton, indicating that the host rock and MMEs did not evolve through the differentiation of major mineral crystallization. If they are co-genetic enclaves, elements such as Sr, Zr, and others in the MME should have higher concentrations than in the host rock. In addition, the relatively high viscosity of granitic melts hinders the effective separation and aggregation of crystals from the melt, which presents a physical barrier to the origin of mineral heap crystals in granite [83].

Condensation margins and complex annular plagioclase can be seen in some MMEs (Figure 2d), indicating that there is a large temperature difference between the MMEs and the host rock, which is the result of rapid condensation [78,84]. Acicular apatite is widely distributed in MMEs (Figure 2f,i), suggesting that the magma-forming MMEs had a large temperature difference compared with the magma of the host rock, and there was a rapid exothermic effect during the crystallization process, indicating magmatic mixing [85–89]. Zircon U-Pb chronology shows that the MMEs of the Liuba pluton have a similar formation age to that of the host rock, which indicates that the MMEs are not the residual bodies from the melting of metamorphic and sedimentary rocks. The chondrite-normalized REE patterns and primitive mantle-normalized trace element spider diagrams also show that the MMEs follow the same evolutionary trend as the host rock (Figure 4a,b), which reflects the possible evolutionary trend of mixing between the host rock and MMEs [9]. In the FeO^T-MgO diagram reflecting the magmatic evolution pattern (Figure 10b), both the Liuba

pluton and the MME samples fall on the mixing trend line, indicating that chemical mixing has occurred [90–92]. The characteristic parameters of the MMEs and host rock are similar, indicating that the MMEs and host rock may be products of homologous or contemporary magmatic evolution. La/Nb (1.04–5.39), with an average of 3.53, is greater than 0.1, which is different from the mantle-derived magma [93]. Rb/Sr (0.08–0.18), with an average of 0.12, is close to the average value of the continental crust (0.24) [94], indicating that the source rocks of the host rock and the MMEs are derived from the continental crust. Based on the above, it can be concluded that the Liuba quartz diorite and dioritic MMEs originated from a common crustal source region. They formed through the mixing of two different types of crustal magma with distinct elemental compositions. The MMEs were formed in relatively high-temperature conditions through partial melting of mafic crustal rocks, generating a neutral magma, which was then injected into the host rock's feldspar magma, leading to magma mixing. During this process, partial aggregation of dark-colored minerals occurred.

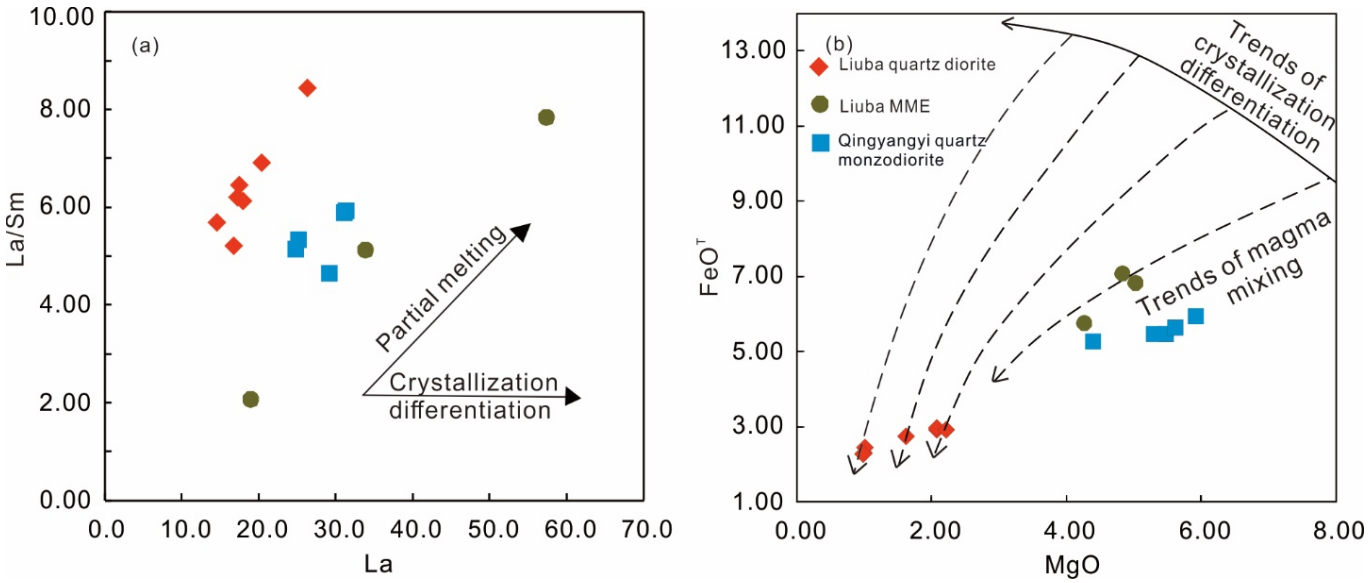


Figure 10. Diagrams of (**a**) La-Sm vs. La and (**b**) FeO^T vs. MgO for Liuba quartz diorite, MMEs and Qingyangyi quartz monzodiorite [85,95].

6.3. Tectonic Setting and Geological Significance

From the perspective of field geological characteristics, the Liuba pluton intrudes into the Silurian lower-grade metamorphic sedimentary strata and the Devonian sedimentary strata on the north side of the Mianlue tectonic belt, and the Qingyangyi pluton intrudes into the northern side of the Mianlue tectonic belt. Both plutons have not been deformed, and their distribution direction is generally consistent with the regional structural line. This suggests that both plutons were formed after the main collision and the regional structural deformation, and their formation should be later than the main deformation period of the Mianlue tectonic belt.

The geochemical characteristics of the Liuba and Qingyangyi plutons show high-K calc-alkaline granite. It is generally believed that high-K calc-alkaline series magmatic rocks are one of the important features of post-collision magmatic activity [96–100]. This suggests that high-K calc-alkaline I-type granites form in island arc or late post-collision environments. In addition, it is generally believed that there are two formation mechanisms for partial melting of the lower crust. One is that during the main orogenic period, the intense compression occurring between continental crusts leads to thickening of the lower crust and internal structural shear. Under the influence of the geothermal gradient, this causes an increase in crustal temperature. Combined with the heat generated by shear

activity, this results in partial melting of the lower crust. The other is that under the action of extension stress after main orogenic period, due to gravitational sinking collapse, the upwelling of mantle materials induces partial melting of the lower crustal materials. In the post-collision stage, this results in the formation of a large amount of high-K calc-alkaline magma [53]. The post-collision granites have higher alkali ($K_2O + Na_2O$) and Sr compared to island arc magmas, with higher ratios of (Fe_2O_3 + FeO)/(MgO) and K_2O/Na_2O as well [101,102]. The Liuba and Qingyangyi plutons are high-K alkaline I-type granites, which have a higher total alkali content compared to island arc magmas (Liuba pluton: 6.17%~7.93%, Qingyangyi pluton: 5.23%~5.66%). They also exhibit higher Zr/Y ratios (7.75~13.9, 4.63~7.13) than the island arc magmatic rocks. On the Rb-Y + Nb diagram (Figure 11a), the data points for the quartz monzodiorite of Qingyangyi pluton and dioritic MMEs of the Liuba pluton fall within the post-collision granite (Post-COLG) region, and the data points of Liuba quartz diorite fall near the Post-COLG region. On the Nb-Y diagram (Figure 11b), all the data points fall within the volcanic arc granite (VAG) and syn-collisional granite (Syn-COLG) regions, indicating that both plutons formed in post-collision environments.

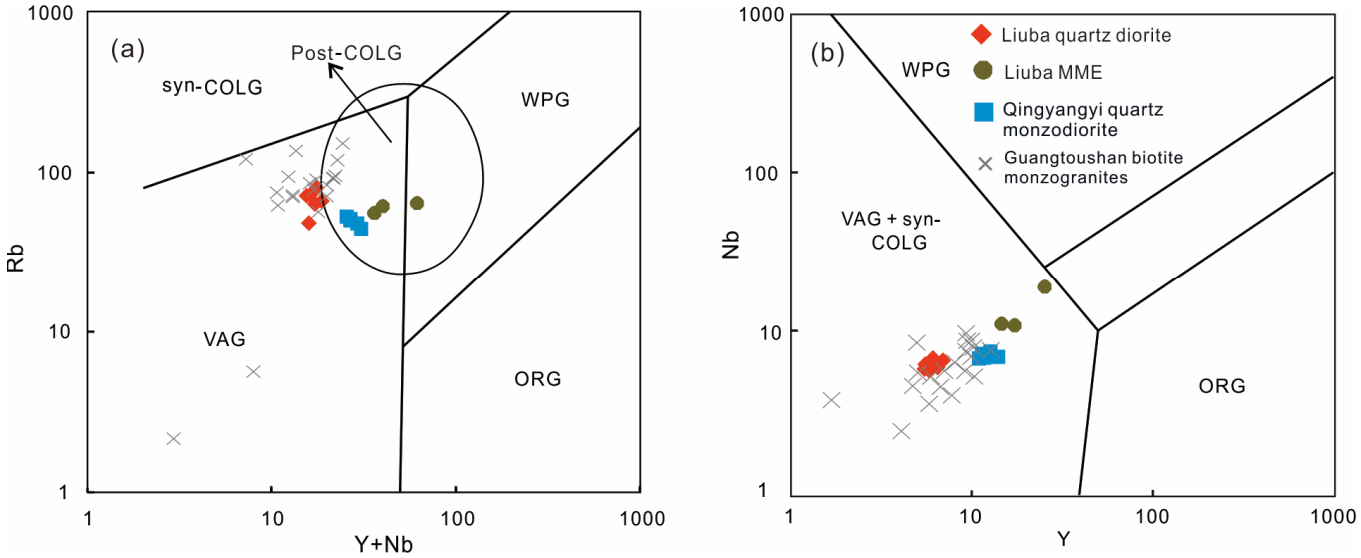


Figure 11. Discrimination diagrams of trace element tectonic environment (**a**) Rb vs. (Y + Nb) (**b**) Nb vs. Y for Liuba quartz diorite, MMEs and Qingyangyi quartz monzodiorite [96].

Current studies suggest that the Yangtze Block and the NCB completed collision in the early Mesozoic, and the collision mainly occurred in 254–220 Ma [2,4,103–109]. The tectonic evolution of the South Qinling tectonic belt occurred in three stages: before the early Triassic, during the subduction phase of the Mianlue Ocean beneath the South Qinling Block; the middle Triassic was the transition stage of Mianlue ocean subduction to continental-continental collision; and the late Triassic was the late adjustment stage of the South Qinling Block entering the collisional orogeny, during which a huge number of late Triassic granite plutons formed. These granite plutons may be the products of the lithosphere of the orogenic belt thickening and undergoing delamination after the peak of the collision orogeny [7,53,72,110]. The Liuba and Qingyangyi pluton emplacement (215 Ma) had ended the subduction in the entire region (254–220 Ma) [4,103]. The formation age of the Liuba and Qingyangyi plutons is 215 Ma, which is in the post-collision stage of the main orogenic period, and the stress state changed from compressive to extensional [4,106,107,111–115]. During this transition stage, the gradual relaxation of compressive stress often resulted in the formation of a large amount of potassium rich calc-alkaline magma [53]. At the same

time, it indicates that the Mianlue Ocean had completely closed before 215 Ma, and the collision orogenic stage between the Yangtze Block and the NCB had entered its late phase, which would subsequently lead to intraplate tectonic activities.

7. Conclusions

Based on the detailed study of the petrology, zircon U-Pb chronology, geochemistry, and tectonic environment of the quartz diorite and MMEs of the Liuba pluton and the quartz monzodiorite of the Qingyangyi pluton in the South Qinling. The conclusions are as follows:

(1) The LA-ICP-MS zircon U-Pb ages of the Liuba quartz diorite, dioritic MMEs, and the Qingyangyi quartz monzodiorite are 216.1 ± 0.8 Ma~217.1 ± 1.3 Ma, 215.4 ± 1.0 Ma, and 214.6 ± 0.9 Ma~215.4 ± 0.9 Ma, respectively, indicating formation during the late Triassic. The ages of formation the quartz diorite host rock and the dioritic MMEs in the Liuba pluton are basically consistent within the error range, which indicates that simultaneous felsic and mafic magmatic activities existed in the South Qinling during the late Triassic.

(2) The quartz diorite and dioritic MMEs in the Liuba pluton are products of a common magmatic evolutionary process. The source rocks of both the Liuba quartz diorite and dioritic MMEs, as well as the Qingyangyi quartz monzodiorite, are likely derived from partial melting of the basic lower crust. The dioritic MMEs are neutral magma produced by partial melting of mafic crustal rocks and then injected into the host rock felsic magma to form magma mixing.

(3) The geological and geochemical characteristics of the Liuba and Qingyangyi plutons indicate that both plutons were formed in the collisional to the post-collisional transformation stage. They are classified as post-orogenic granites, resulting from the comprehensive collision between the Yangtze Block and NCB, leading to crustal thickening and partial melting of the lower crust. This reflects the magmatic intrusion activities during the late Triassic period along the Mianlue tectonic belt in the South Qinling tectonic belt.

Supplementary Materials: The following supporting information can be downloaded at: https://www.mdpi.com/article/10.3390/min15010077/s1, Supplementary Table S1: Analytical results of Liuba and Qingyangyi plutons for major elements (Wt%) and trace elements (ppm); Supplementary Table S2: LA-ICP MS zircon U-Pb dating results of Liuba and Qingyangyi plutons.

Author Contributions: Conceptualization, S.G. and X.P.; methodology, S.G. and X.P.; software, X.L and S.G.; validation, S.G. and X.P.; formal analysis, S.G., Z.L., X.P. and R.L.; investigation, S.G., Z.L., X.W., X.P., S.Z., L.P., L.Q. and M.W.; resources, R.L., Z.L. and X.P.; data curation, S.G. and X.P.; writing-original draft preparation, S.G. and X.P.; writing-review and editing, S.G., R.L. and X.P.; visualization, S.G.; supervision, Z.L., R.L. and X.P.; project administration, Z.L., X.P. and R.L.; funding acquisition, Z.L., X.P. and R.L. All authors have read and agreed to the published version of the manuscript.

Funding: This research was funded by the National Natural Science Foundation of China (Grant Nos. 42472272, 41872233, 42172236, 41472191, 41502191, 41872235), and the Youth Innovation Team of Shaanxi Universities.

Data Availability Statement: The original contributions presented in the study are included in the article/Supplementary Materials.

Acknowledgments: The authors thank X.P. and the teachers for their contributions, which have improved the completion of this paper. The authors thank the anonymous reviewers for their critical comments, which greatly improved the quality of this paper.

Conflicts of Interest: The authors declare no conflicts of interest.

References

1. Ratschbacher, L.; Hacker, B.R.; Calvert, A.; Webb, L.E.; Grimmer, J.C.; McWilliams, M.O.; Ireland, T.; Dong, S.W.; Hu, J.M. Tectonics of the Qinling (Central China): Tectonostratigraphy, Geochronology, and Deformation History. *Tectonophysics* **2003**, *366*, 1–53. [CrossRef]
2. Zhang, G.W.; Dong, Y.P.; Yao, A.P. Review on the development of studies on the tectonic and orogen process of orogenic belt, and discussing on some new key problems. *Northwest. Geol.* **2001**, *34*, 1–9. (In Chinese)
3. Zhang, G.W.; Zhang, Z.Q.; Dong, Y.P. Nature of Main Tectono-Lithostratigraphic units of the Qinling Orogen: Implications for the tectionic evolution. *Acta Petrol. Sin.* **1995**, *11*, 101–114. (In Chinese)
4. Li, S.G.; Sun, W.D.; Zhang, G.W.; Chen, J.Y.; Yang, Y.C. Chronology and geochemistry of metamorphic volcanic rocks in the Heigouxia zone of the Southern Qinling: Evidence for the Paleozoic ocean basin and its closure age. *Sci. China Ser. D Earth Sci.* **1996**, *26*, 223–230. (In Chinese)
5. Lu, S.N.; Chen, Z.H.; Li, H.K.; Hao, G.J.; Zhou, H.Y.; Xiang, Z.Q. Late Mesoproteroroic-early Neoproterozoic evolution of the Qinling orogen. *Geol. Bull. China* **2004**, *23*, 107–112. (In Chinese)
6. Zhang, C.L.; Liu, L.; Zhang, G.W.; Wang, T.; Chen, D.L.; Yuan, H.L.; Liu, X.M.; Yan, Y.X. Determination of Neoproterozoic post-collisional granitesin the north Qinling Mountains and its tectonic significance. *Front. Earth Sci.* **2004**, *11*, 33–42. (In Chinese)
7. Zhang, C.L.; Wang, T.; Wang, X.X. Origin and tectonic setting of the early Mesozoic granitoids in Qinling Orogenic Belt. *J. Geol.* **2008**, *14*, 304–316. (In Chinese)
8. Meng, Q.R.; Zhang, G.W. Timing of collision of the north and South China Blocks: Controversy and reconciliation. *Geology* **1999**, *27*, 123–126. (In Chinese) [CrossRef]
9. Li, Z.C.; Pei, X.Z.; Li, R.B.; Pei, L.; Hu, B.; Liu, C.J.; Chen, G.C.; Chen, Y.X. LA-ICP-MS zircon U-Pb dating, geochemistry of the Mishuling intrusion in western Qinling and their tectonic significance. *Acta Petrol. Sin.* **2013**, *29*, 2617–2634. (In Chinese)
10. Zhang, G.W.; Guo, A.L.; Dong, Y.P.; Yao, A.P. Rethinking of the Qinling Orogen. *J. Geomech.* **2019**, *25*, 746–768. (In Chinese)
11. Li, Y. Emplacement Mechanism and Its Tectonic Implications of the Dongjiangkou Pluton, Qinling Orogen. Doctor Thesis, Northwest University, Xi'an, China, 2017. (In Chinese).
12. Meng, X.Y.; Wang, X.X.; Ke, C.H.; Li, J.B.; Yang, Y.; Lü, X.Q. Geochemistry and Hf isotope of the granitoids from Huayang pluton in South Qinling orogen: Constraints on the genesis of Wulong plutons. *Geol. Bull. China.* **2013**, *32*, 1704–1719. (In Chinese)
13. Huang, Q.W.; Shi, Y.; Liu, M.H.; Liu, X.J.; Bai, Z.A.; Qin, K.L. Geochronology and Geochemistry of the Shahewan and Caoping granites in South Qinling and their significance. *Earth Sci.* **2018**, *43*, 81–102.
14. Shaanxi Geological Survey Institute. *Regional Geology of China: Shaanxi Volume*; Geological Publishing House: Beijing, China, 2017. (In Chinese)
15. Xu, X.Y.; Chen, J.L.; Yan, Z.; Wang, R.Y.; Li, P.; Li, T.; Wang, H.L.; Yang, Y.Z.; Yang, J.L.; Li, Z.P.; et al. *Geological Map of the Qinling and Adjacent Areas (1:500,000)*; Xi'an Map Publishing House: Xi'an, China, 2014. (In Chinese)
16. Sun, W.D.; Li, S.G.; Chen, Y.; Li, Y. U-Pb Dating of zircon from South Qinling granitoids and its geological significance. *Geochemistry* **2000**, *29*, 209–216. (In Chinese)
17. Zhang, G.W.; Dong, Y.P.; Lai, S.C.; Guo, A.L.; Meng, Q.R.; Liu, S.F.; Cheng, S.Y.; Yao, A.P.; Zhang, Z.Q.; Pei, X.Z.; et al. The Mianlue tectonic zone and Mianlue suture zone on southern margin of the Qinling-Dabie Orogenic Belt. *Sci. China Ser. D Earth Sci.* **2003**, *33*, 1121–1135. (In Chinese)
18. Sun, W.; Li, S.; Chen, Y.; Li, Y. Timing of synorogenic granitoids in the South Qinling, Central China: Constraints on the evolution of the Qinling-Dabie Orogenic Belt. *J. Geol.* **2002**, *110*, 457–468. [CrossRef]
19. Wang, X.X.; Wang, T.; Zhang, C.L. Neoproterozoic, Paleozoic, and mesozoic granitoid magmatism in the Qinling orogen, China: Constraints on orogenic process. *J. Asian Earth Sci.* **2013**, *72*, 129–151. [CrossRef]
20. Zhang, G.W.; Meng, Q.R.; Lai, S. Tectonics and structure of the Qinling Orogenic Belt. *Sci. China Ser. D Earth Sci.* **1995**, *25*, 994–1003.
21. Zhang, G.W.; Zhang, B.R.; Yuan, X.C.; Xiao, Q.H. *Qinling Orogenic Belt and Continental Geodynamics*; Beijing Science Press: Beijing, China, 2001. (In Chinese)
22. Dong, Y.P.; Zhang, G.W.; Zhao, X.; Yao, A.P.; Liu, X.M. Geochemistry of the subduction-related magmatic rocks in the Dahong mountains, Northern Hubei Province. *Sci. China Earth Sci.* **2004**, *47*, 366–377. [CrossRef]
23. Pei, X.Z.; Wang, T.; Li, W.P.; Zhang, W.J.; Wang, Q.Q.; Li, G.G. Tectonic and magmatic evolution characteristics in the Shangdan area of North Qinling. *Northwest. Geol.* **1995**, *16*, 13–19. (In Chinese)
24. Pei, X.Z.; Zhang, G.W.; Lai, S.C.; Li, Y.; Chen, L.; Gao, M. Main geological features of the Mianlue tectonic belt on the southern margin of the West Qinling. *Geol. Bull.* **2002**, *21*, 486–494. (In Chinese)
25. Mattauer, P.; Malavieille, J.; Tapponnier, P.; Maluski, H.; Xu, Z.Q.; Lu, Y.L.; Tang, Y.Q. Tectonics of the Qinling belt: Build-up and evolution of Eastern Asia. *Nature* **1985**, *317*, 496–500. [CrossRef]

26. Meng, Q.R.; Zhang, G.W. Geologic framework and tectonic evolution of the Qinling orogen, Central China. *Tectonophysics* **2000**, *323*, 183–196. [CrossRef]
27. Chen, F.; Hegner, E.; Todt, W. Zircon ages and Nd isotopic and chemical compositions of orthogneisses from the black forest, Germany: Evidence for a cambrian magmatic arc. *Int. J. Earth Sci.* **2000**, *88*, 791–802. [CrossRef]
28. *GB/T 14506.28–2010*; Methods for Chemical Analysis of Silicate Rocks—Part 28: Determination of 16 Major and Minor Elements Content. China Standards Press: Beijing, China, 2010.
29. Luan, Y.; He, K.; Tan, X.J. In situ U-Pb dating and trace element determination of standard zircons by LA-ICP-MS. *Geol. Bull. China* **2019**, *38*, 1206–1218.
30. Hu, Z.C.; Zhang, W.; Liu, Y.S.; Gao, S.; Li, M.; Zong, K.Q.; Chen, H.H.; Hu, S.H. "Wave" signal smoothing and mercury removing device for laser ablation quadrupole and multiple collector ICP-MS analysis: Application to lead isotope analysis. *Anal. Chem.* **2015**, *87*, 1152–1157. [CrossRef] [PubMed]
31. Liu, Y.S.; Hu, Z.C.; Gao, S.; Gunther, D.; Xu, J.; Gao, C.G.; Chen, H.H. In situ analysis of major and trace elements of anhydrous minerals by LA-ICP-MS without applying an internalstandard. *Chem. Geol.* **2008**, *257*, 34–43. [CrossRef]
32. Liu, Y.S.; Gao, S.; Hu, Z.C.; Gao, C.G.; Zong, K.Q.; Wang, D.B. Continental and oceanic crust recycling-induced melt-peridotite interactions in the Trans-North China Orogen: U-Pb dating, Hf isotopes and trace elements in zircons of mantle xenoliths. *J. Petrol.* **2010**, *51*, 537–571. [CrossRef]
33. Le Maitre, R.W. *A Classification of Igneous Rocks and Glossary of Terms: Recommendations of the International Union of Geological Sciences Subcommission on the Systematics of Igneous Rocks*; Blackwell: Oxford, UK, 1989.
34. Middlemost, E.A.K. Naming materials in the magma/igneous rock system. *Earth Sci. Rev.* **1994**, *37*, 215–224. [CrossRef]
35. Rickwood, P.C. Boundary lines within petrologic diagrams which use oxides of major and minor elements. *Lithos* **1989**, *22*, 247–263. [CrossRef]
36. Frost, B.R.; Barnes, C.G.; Collins, W.J.; Arculus, R.J.; Ellis, D.J.; Frost, C.D. A geochemical classification for granitic rocks. *J. Petrol.* **2001**, *42*, 2033–2048. [CrossRef]
37. Guan, Q.; Cao, J.L.; Wang, R.X.; Xie, P.L.; Xia, W.Y.; Li, X.W. Petrological and Geochemical Constraints on the Origin of Strongly Peraluminous Granitoids from the Triassic Guangtoushan Pluton in South Qinling. *Acta. Geol Sin. Engl.* **2023**, *97*, 1683–1697. [CrossRef]
38. Liu, S.W.; Li, Q.G.; Tian, W.; Wang, Z.Q.; Yang, P.T.; Wang, Z.; Wei, B.X.; Guo, R.R. Petrogenesis of Indosinian Granitoids in Middle-Segment of South Qinling Tectonic Belt: Constraints from Sr-Nd Isotopie Systematies. *Acta. Geol. Sin. Engl.* **2011**, *85*, 610–628. [CrossRef]
39. Sun, S.S.; McDonough, W.F. Chemical and isotopic systematics of oceanic basalts: Implications for mantle composition and processes. *Geol. Soc. Spec. Publ.* **1989**, *42*, 313–345. [CrossRef]
40. Zhang, C.L.; Luo, J.L.; Li, M.; Wang, Y. Geochemical characteristics and geological significance of Xiba granite, porphyrite in East Qinling. *J. Northwest Univ. Nat. Sci. Ed.* **2002**, *32*, 374–388.
41. Corfu, F.; Hanchar, J.M.; Hoskin, P.W.O.; Kinny, P. Atlas of zircon textures. *Rev. Mineral. Geochem.* **2003**, *53*, 469–500. [CrossRef]
42. Belousova, E.; Griffin, W.L.; O'Reilly, S.Y.; Fisher, N. Igneous zircon: Trace element composition as an indicator of source rock type. *Contrib. Mineral. Petrol.* **2002**, *143*, 602–622. [CrossRef]
43. Wu, Y.B.; Zheng, Y.F. The mineralogical study of zircon genesis and its constraints on U-Pb age interpretation. *Chin. Sci. Bull.* **2004**, *49*, 1589–1604. (In Chinese) [CrossRef]
44. Taylor, S.R.; McLennan, S.M. The geochemical evolution of the continental crust. *Rev. Geophys.* **1995**, *33*, 241–265. [CrossRef]
45. Patiño Douce, A.E. What do experiments tell us about therelative contributions of crust and mantle to the origin of granitic magmas? *Geol. Soc. Spec. Publ.* **1999**, *168*, 55–75. [CrossRef]
46. Kaygusuz, A.; Siebel, W.; Ilbeyli, N.; Arslan, M.; Satır, M.; Sen, C. Insight into magma genesis at convergent plate margins-A case study from the eastern Pontides (NE Turkey). *Neues Jahrb. Fur Miner.* **2010**, *187*, 265–287. [CrossRef]
47. Rapp, R.P.; Watson, E.B. Dehydration melting of metabasalt at 8–32 kbar: Implications for continental growth and crust-mantle recycling. *J. Petrol.* **1995**, *36*, 891–931. [CrossRef]
48. Yan, Q.R.; Wang, Z.Q.; Yan, Z.; Xiang, Z.J.; Chen, J.L.; Wang, T. SHRIMP analyses for ophiolitic—Mafic blocks in the Kangxian—Mianxian section of the Mianxian—Lueyang melange: Their geological implications. *Geol. Rev.* **2007**, *53*, 755–764. (In Chinese)
49. Zhao, Z.H.; Xiong, X.L.; Wang, Q.; Qiao, Y.L. Some geochemical issues on Nb and Ta. *Geochimica* **2008**, *37*, 304–320. (In Chinese)
50. Hofmann, A.W. Chemical differentiation of the Earth: The relationship between mantle, continental crust, and oceanic crust. *Earth Planet. Sci. Lett.* **1988**, *90*, 297–314. [CrossRef]
51. Gao, Y.F.; Hou, Z.Q.; Wei, R.H. Neogene porphyries from Gangdese: Petrological, geochemical characteristics and geodynamic significances. *Acta Petrol. Sin.* **2003**, *19*, 418–428. (In Chinese)
52. Wilson, M. *Igneous Petrogenesis: A Global Tectonic Approach*; Unwin Hyman: London, UK, 1989.

53. Zhang, C.L.; Zhang, G.W.; Yan, Y.X.; Wang, Y.C. Origin and dynamic significance of Guangtoushan granitic plutons to the north of Mianlue zone in southern Qinling. *Acta Petrol. Sin.* **2005**, *21*, 711–720. (In Chinese)
54. Yang, P.T.; Liu, S.W.; Li, Q.G.; Wang, Z.Q.; Zhang, F.; Wang, W. Chronology and petrogenesis of the Hejiazhuang granitoid pluton and its constraints on the Early Triassic tectonic evolution of the South Qinling Belt. *Sci. China Ser. D Earth Sci.* **2013**, *43*, 1874–1893. (In Chinese) [CrossRef]
55. Zhang, F.; Liu, S.W.; Li, Q.G.; Wang, Z.Q.; Han, Y.G.; Yang, K.; Wu, F. LA-ICP-MS zircon U-Pb geochronology and geological significance of Xiba granitoids from Qinling, Central China. *Acta Sci. Nat. Univ. Pekin.* **2009**, *45*, 833–840. (In Chinese)
56. Zhang, Y.F.; Yang, T.; Yi, P.F.; Yao, Z.; He, Y.F. LA—ICP—MS zircon geochro-nology and geochemistry of the Huahongshuping granodiorite pluton in south Qinling. *Geol. Explor.* **2018**, *54*, 300–314. (In Chinese)
57. Yi, P.F.; Zhang, Y.F.; Zhang, G.L.; Yang, T.; Yao, Z.; Li, Q.; Gao, H.F. LA-ICP-MS Zircon U-Pb Ages, Geochemical characteristics of Zaomulan Granitic pluton in southern Qinling Orogenic Belt and their geological implications. *Geol. Rev.* **2017**, *63*, 1497–1511. (In Chinese)
58. Wang, X.X.; Wang, T.; Happala, L.; Lu, X.X. Genesis of mafic enclaves from rapakivi-textured granites in the Qinling and its petrological significance: Evidence of elements and Nd, Sr isotopes. *Acta Petrol. Sin.* **2005**, *21*, 935–946. (In Chinese)
59. Wang, X.X.; Wang, T.; Qi, Q.J.; Li, S. Temporal-spatial variations, origin and their tectonic significance of the Late Mesozoic granites in the Qinling, Central China. *Acta Petrol. Sin.* **2011**, *27*, 1573–1593. (In Chinese)
60. Wang, X.X.; Wang, T.; Zhang, C.L. Granitoid magmatism in the Qinling orogeny, central China and its bearing on orogenic evolution. *Sci. China Earth Sci.* **2015**, *45*, 1109–1125. (In Chinese)
61. Zhang, H.F.; Zhang, B.R.; Ling, W.L.; Gao, S.; Ouyang, J.P. Late Proterozoic crustal accretion of south Qinling: Nd isotopic study from granitic rocks. *Geochimica* **1997**, *26*, 16–24. (In Chinese)
62. Zhang, H.F.; Jin, L.L.; Zhang, L.; Nigel, H.; Zhou, L.; Hu, S.H.; Zhang, B.R. Geochemistry of granites in the Western Qinling and their Pb-Sr-Nd isotopic compositions as constraints on the basement properties and tectonic attributes. *Sci. China Ser. D Earth Sci.* **2005**, *35*, 10–22. (In Chinese)
63. Zhang, H.F.; Xiao, L.; Zhang, L.; Yuan, H.L.; Jin, L.L. Geochemistry and Pb-Sr-Nd isotopic compositions of Indosinian granites in the Bikou block, northwestern margin of the Yangtze Craton: Constraints on rock genesis and dynamic background. *Sci. China Ser. D Earth Sci.* **2007**, *37*, 460–470. (In Chinese)
64. Roberts, M.P.; Clemens, J.D. Origin of high-potassium, calc-alkaline, I-type granitoids. *Geology* **1993**, *21*, 825–828. [CrossRef]
65. Zhang, C.L.; Zhou, D.W.; Jin, H.L.; Han, S.; Liu, Y.Y. Study on the Sr, Nd, Pb and O isotopes of basic dyke swarms in the Wudang block and basic volcanics of the Yaolinghe Group. *Acta Petrol. Sin.* **1999**, *15*, 430–437. (In Chinese) [CrossRef]
66. Ling, W.; Gao, S.; Zhang, B.R.; Li, H.M.; Liu, Y.; Cheng, J.P. Neoproterozoic tectonic evolution of the northwestern Yangtze craton, South China: Implications for amalgamation and break-up of the Rodinia Supercontinent. *Precambrian Res.* **2003**, *122*, 111–140. [CrossRef]
67. Xia, L.Q.; Xia, Z.C.; Xu, X.Y.; Li, X.M.; Ma, Z.P. Petrogenesis of the Bikou Group volcanic rocks. *Front. Earth Sci.* **2007**, *14*, 84–101. (In Chinese)
68. Xia, L.Q.; Xia, Z.C.; Li, X.M.; Ma, Z.P.; Xu, X.Y. Petrogenesis of the Yaolinghe Group, Yunxi Group, Wudangshan Group Volcanic rocks and basic dyke swarms from eastern part of the South Qinling Mountains. *Northwest. Geol.* **2008**, *41*, 1–29. (In Chinese)
69. Xia, L.Q.; Xia, Z.C.; Ma, Z.P.; Xu, X.Y.; Li, X.M. Petrogenesis of volcanic rocks from Xixiang Group in middle part of South Qinling Mountains. *Northwest. Geol.* **2009**, *42*, 1–37. (In Chinese)
70. Ling, W.; Ren, B.F.; Duan, R.C.; Liu, X.M.; Mao, X.W.; Peng, L.H.; Liu, Z.X.; Cheng, J.P.; Yang, H.M. Zircon U-Pb isotopic dating of the Wudangshan Group, Yaoling River Group, and basic intrusive rock group in the South Qinling and its geological significance. *Sci. Bull.* **2007**, *52*, 1445–1456. (In Chinese)
71. Li, Y.F.; Lai, S.C.; Qin, J.F.; Liu, X.; Wang, J. Geochemical characteristics and Sr-Nd-Pb isotopic compositions of the Bikou volcanic rock series: Evidence for the rifting of the northern margin of the Yangtze Block during the Jinning period. *Sci. China Ser. D Earth Sci.* **2007**, *37*, 295–306. (In Chinese)
72. Qin, J.F. Petrogenesis and Geodynamic Implications of the Late-Triassic Granitoids from the Qinling Orogenic Belt. Doctor Thesis, Northwest University, Xi'an, China, 2010. (In Chinese).
73. Zhang, B.R.; Gao, S.; Zhang, H.F.; Han, Y.W. *Geochemistry of the Qinling Orogen*; Science Press: Beijing, China, 2002. (In Chinese)
74. Chappell, B.W.; Wyborn, D. Peraluminous I-type granites. *Lithos* **2012**, *153*, 142–153. [CrossRef]
75. Noyes, H.J.; Frey, F.A.; Wones, D.R. A tale of two plutons: Geochemical evidence bearing on the origin and differentiation of the Red Lake and Eagle Peak plutons, Central Sierra Nevada, California. *J. Geol.* **1983**, *91*, 487–509. [CrossRef]
76. Clemens, J.D.; Wall, V.J. Controls on the mineralogy of S-type volcanic and plutonic rocks. *Lithos* **1988**, *21*, 53–66. [CrossRef]
77. Shellnutt, J.G.; Jahn, B.M.; Dostal, J. Elemental and Sr–Nd isotope geochemistry of microgranular enclaves from peralkaline A-type granitic plutons of the Emeishan large igneous province, SW China. *Lithos* **2010**, *119*, 34–46. [CrossRef]
78. Kumar, S.; Rino, V.; Pal, A.B. Field evidence of magma mixing from microgranular enclaves hosted in Palaeoproterozoic Malanjkh and granitoids, Central India. *Gondwana Res.* **2004**, *7*, 539–548. [CrossRef]

79. Barbarin, B. Mafic magmatic enclaves and mafic rocks associated with some granitoids of the central Sierra Nevada batholith, California: Nature, origin, and relations with the hosts. *Lithos* **2005**, *80*, 155–177. [CrossRef]
80. Clemens, J.; Stevens, G. What controls chemical variation in granitic magmas? *Lithos* **2012**, *134*, 317–329. [CrossRef]
81. Chappell, B.W.; White, A.J.R. I- and S-type granites in the Lachlan Fold Belt. *Earth Environ. Sci. Trans. R. Soc. Edinb.* **1992**, *83*, 1–26.
82. White, R.V.; Tarney, J.; Kerr, A.C.; Saunders, A.D.; Kempton, P.D.; Pringle, M.S.; Klaver, G.T. Modification of an oceanic plateau, Aruba, Dutch Caribbean: Implications for the generation of continental crust. *Lithos* **1999**, *46*, 43–68. [CrossRef]
83. Donaire, T.; Pascual, E.; Pin, C.; Duthou, J.L. Microgranular Enclaves as evidence of rapid cooling in granitoid rocks: The case of the Los Pedroches granodiorite, iberian massif, Spain. *Contrib. Mineral. Petrol.* **2005**, *149*, 247–265. [CrossRef]
84. Wiebe, R.A.; Smith, D.; Sturm, M.; King, E.M.; Seckler, M.S. Enclaves in the Cadillac Mountain granite (Coastal Maine): Samples of hybrid magma from the base of the chamber. *J. Petrol.* **1997**, *38*, 393–423. [CrossRef]
85. Wyllie, M.R.J.; Gardner, G.H.F.; Gregory, A.R. Studies of elastic wave attenuation in porous media. *Geophysics* **1962**, *27*, 569–589. [CrossRef]
86. Zorpi, M.J.; Coulon, C.; Orsini, J.B.; Cocirta, C. Magma mingling, zoning and emplacement in calc-alkaline granitoid plutons. *Tectonophysics* **1989**, *157*, 315–329. [CrossRef]
87. Barbarin, B. Field evidence for successive mixing and mingling between the piolard diorite and the Saint-Julien-la-VêtreMonzogranite (Nord–Forez, Massif Central, France). *Can. J. Earth Sci.* **1988**, *25*, 49–59. [CrossRef]
88. Barbarin, B.; Didier, J. Genesis and Evolution of mafic microgranular enclaves through various types of interaction between coexisting felsic and mafic magmas. *Earth Environ. Sci. Trans. R. Soc. Edinb.* **1992**, *8*, 145–153.
89. Baxter, S.; Feely, M. Magma mixing and mingling textures in granitoids: Examples from the galway granite, connemara, Ireland. *Mineral. Petrol.* **2002**, *76*, 63–74. [CrossRef]
90. Castro, A.; Moreno-Ventas, I.; De La Rosa, J. H-type (Hybrid) Granitoids: A proposed revision of the granite-type classification and nomenclature. *Earth Sci. Rev.* **1991**, *31*, 237–253. [CrossRef]
91. Qu, X.M.; Wang, H.N. Dynamics study on the crustal-mantle magma mixing and emplacement mechanism of Guojialin granite. *Sci. Geol. Sin.* **1997**, *32*, 445–454. (In Chinese)
92. Jiang, W.; Mo, X.X.; Zhao, C.H.; Guo, T.Y.; Zhang, S.Q. Geochemistry of granitoid and its mafic microgranular enclave in Gangdise belt, Qinghai-Xizang Plateau. *Acta Petrol. Sin.* **1999**, *15*, 90–98. (In Chinese)
93. DePaolo, D.J.; Daley, E.E. Neodymium isotopes in basalts of the southwest basin and range and lithospheric thinning during continental extension. *Chem. Geol.* **2000**, *169*, 157–185. [CrossRef]
94. Taylor, S.R.; McLennan, S.M. *The Continental Crust: Its Composition and Evolution*; Blackwell Scientific Publication: Oxford, UK, 1985; p. 132.
95. Keppler, H. Constraints from partitioning experiments on the composition of subduction-zone fluids. *Nature* **1996**, *380*, 237–240. [CrossRef]
96. Pearce, J.A.; Harris, N.B.W.; Tindle, A.G. Trace element discrimination diagrams for the tectonic interpretation of granitic rocks. *J. Petrol.* **1984**, *25*, 956–983. [CrossRef]
97. Pearce, J.A. Sources and settings of granitic rocks. *Episodes* **1996**, *19*, 120–125. [CrossRef]
98. Pitcher, W.S. The nature and origin of granite. *Blackie Acad. Prof.* **1993**, 1–321.
99. Bonin, B. Do coeval mafic and felsic magmas in post-collisional to within-plate regimes necessarily imply two contrasting, mantle and crustal, sources? A review. *Lithos* **2004**, *78*, 1–24. [CrossRef]
100. Clemens, J.; Darbyshire, D.; Flinders, J. Sources of post-orogenic calc-alkaline magmas: The Arrochar and Garabal Hill–Glen Fyne complexes, Scotland. *Lithos* **2009**, *112*, 524–542. [CrossRef]
101. Elburg, M.A.; Foden, J. Geochemical response to varying tectonic settings: An example from southern Sulawesi (Indonesia). *Geochim. Cosmochim. Acta* **1999**, *63*, 1155–1172. [CrossRef]
102. Li, X.Y.; Guo, F.; Wang, Y.J. Post-orogenic tectono-magmatism and its implications for evolution of Orogenic Belts. *Geol. J.* **2002**, *8*, 11. (In Chinese)
103. Hacker, B.R.; Ratschbacher, L.; Webb, L.; Ireland, T.; Walker, D.; Shuwen, D. U/Pb zircon ages constrain the architecture of the ultrahigh-pressure Qinling–Dabie Orogen, China. *Earth Planet. Sci. Lett.* **1998**, *161*, 215–230. [CrossRef]
104. Zhang, H.F.; Gao, S.; Zhang, B.R.; Zhong, Z.Q.; Jia, W.L.; Wang, L.S. Pb isotopic study on crustal structure of Dabie Mountains, central China. *Geochimica* **2001**, *30*, 395–401. (In Chinese)
105. Zheng, Y.F. Advances in research on ultrahigh-pressure metamorphism and continental collision: A case study of the Dabie-Sulu Orogen. *Chin. Sci. Bull.* **2008**, *53*, 2129–2152. (In Chinese) [CrossRef]
106. Dong, Y.P.; Zhang, G.W.; Neubauer, F.; Liu, X.M.; Genser, J.; Hauzenberger, C. Tectonic evolution of the Qinling Orogen, China: Review and synthesis. *J. Asian Earth Sci.* **2011**, *41*, 213–237. [CrossRef]
107. Dong, Y.P.; Liu, X.M.; Zhang, G.W.; Chen, Q.; Zhang, X.N.; Li, W.; Yang, C. Triassic diorites and granitoids in the Foping area: Constraints on the conversion from subduction to collision in the Qinling Orogen, China. *J. Asian Earth Sci.* **2012**, *47*, 123–142. [CrossRef]

108. Gao, F.; Pei, X.Z.; Li, R.B.; Li, Z.C.; Pei, L.; Chen, Y.X.; Wang, M.; Zhao, S.W.; Liu, C.J.; Li, X.B. Neoproterozoic tectonic evolution of the northwestern margin of the Yangtze Block (southwestern China): Evidence from sandstone geochemistry and detrital zircon U–Pb ages of the Hengdan Group. *Precambrian Res.* **2020**, *344*, 105737. [CrossRef]
109. Gao, F.; Pei, X.Z.; Li, R.B.; Li, Z.C.; Pei, L.; Chen, Y.X.; Wang, M.; Zhao, S.W.; Liu, C.J.; Li, X.B. Further constraints on a Neoproterozoic active continental margin from sandstones of the Hengdan Group in the Bikou Terrane, northwestern margin of the Yangtze Block, South China. *J. Asian Earth Sci.* **2020**, *203*, 104514. [CrossRef]
110. Dong, Y.P.; Santosh, M. Tectonic architecture and multiple orogeny of the Qinling Orogenic Belt, Central China. *Gondwana Res.* **2016**, *29*, 1–40. [CrossRef]
111. Yin, Q.; Jagoutz, E.; Kroner, A. Precambrian blueschist/eclogite-bearing belt in central China. *Terra Abstr.* **1991**, *3*, 85–86.
112. Hu, F.Y.; Ducea, M.N.; Liu, S.W.; Chapman, J.B. Quantifying crustal thickness in continental collisional belts: Global perspective and a geologic application. *Sci. Rep.* **2017**, *7*, 7058. [CrossRef] [PubMed]
113. Zhang, H.F.; Zhang, B.R.; Zhao, Z.D.; Luo, T.C. Crustal subduction and collision of the Shangdan tectonic belt in Eastern Qinling: Isotopic tracing evidence from granitic magma source region. *Sci. China Ser. D Earth Sci.* **1996**, *26*, 231–236. (In Chinese)
114. Lu, X.X.; Wei, X.D.; Xiao, Q.H.; Zhang, Z.Q.; Li, H.M.; Wang, W. Geochronological studies of rapakivi granites in Qinling and its geological implications. *Geol. J. China Univ.* **1999**, *5*, 372–377. (In Chinese)
115. Lai, S.C.; Zhang, G.W.; Pei, X.Z.; Yang, H.F. Geochemistry and tectonic significance of the ophiolitic mélange and island arc volcanic rocks in the South Qinling region. *Sci. China Ser. D Earth Sci.* **2003**, *33*, 10–19. (In Chinese)

Disclaimer/Publisher's Note: The statements, opinions and data contained in all publications are solely those of the individual author(s) and contributor(s) and not of MDPI and/or the editor(s). MDPI and/or the editor(s) disclaim responsibility for any injury to people or property resulting from any ideas, methods, instructions or products referred to in the content.